Physics of the Earth and Planetary Interiors 173 (2009) 75–102

Contents lists available at ScienceDirect

Physics of the Earth and Planetary Interiors

journal homepage: www.elsevier.com/locate/pepi

Microwave palaeointensity results from the Matuyama–Brunhes geomagnetic field reversal

Maxwell C. Brown[a,*], Martin N. Gratton[a], John Shaw[a], Richard Holme[a], Vicente Soler[b]

[a] Geomagnetism Laboratory, Department of Earth and Ocean Sciences, Oliver Lodge Building, Oxford Street, University of Liverpool, Liverpool L69 7ZE, United Kingdom
[b] Estación Volcanológica, Instituto de Productos Naturales (CSIC), Avda. Astr. Fco. Sanchez 3, 38206 La Laguna, Tenerife, Spain

ARTICLE INFO

Article history:
Received 7 October 2008
Accepted 9 November 2008

Keywords:
Matuyama–Brunhes
Reversals
Microwave
Palaeomagnetism
Palaeointensity
La Palma
Guadeloupe

ABSTRACT

We present new palaeointensity and palaeodirectional results from the Matuyama–Brunhes geomagnetic field reversal. Volcanic sequences from La Palma and Guadeloupe record the Matuyama–Brunhes boundary, possible precursors, and fluctuations in the magnetic field prior to the main polarity reversal. Absolute palaeointensity was determined using the microwave technique and palaeodirectional results were obtained from thermal demagnetisation. Ten flows from the 29 flows studied gave reliable mean palaeointensities; however, only 1 of the 10 flows records a transitional direction. The VDM determined from this flow is $1.9 \pm 0.6\,(\pm\sigma) \times 10^{22}$ A m^2. Analysis of all Matuyama–Brunhes data suggests that the main directional changes occurred once the VDM was reduced below 3×10^{22} A m^2 (~35% of the present field value).

1. Introduction

The behaviour of the geomagnetic field during reversals is unclear. Understanding the global temporal evolution of the geomagnetic field during reversals can provide important constraints on conditions at the core-mantle boundary and on geodynamo processes (Olson and Amit, 2006). Many palaeomagnetic studies from both sedimentary and lava sequences have sought to uncover details of the reversal process. To fully characterise the behaviour of the geomagnetic field the full magnetic vector must be calculated, requiring both directional and intensity data. Sedimentary sequences provide a quasi-continuous record of directional changes (Coe and Glen, 2004), but lack absolute palaeointensity data. Volcanic records can provide both palaeodirection and absolute palaeointensity; however, they only record fragmentary behaviour of the field at one location on the Earth's surface and where multiple records exist it is extremely difficult to correlate them temporally and establish features globally (Constable, 1990; Gubbins, 1999; Brown et al., 2007; Leonhardt and Fabian, 2007).

The fidelity of both sedimentary and volcanic records is of concern. Problems affecting sedimentary records include: secondary magnetic overprints that can be difficult to remove (Valet et al., 1988); smoothing of the geomagnetic signal caused by low sedimentation rates (Channell and Lehman, 1997; Channell et al., 2004) or to delayed NRM acquisition related to diagenesis and grain growth chemical-remanence mechanisms (Langereis et al., 1992; van Hoof et al., 1993); shallowing of inclination (Celaya and Clement, 1988; Barton and McFadden, 1996; Tauxe and Kent, 2004; Tan et al., 2007); and drilling induced remanence (Fuller and Hasted, 1997).

Determining absolute palaeointensity from volcanic rocks is also problematic, the accuracy of determinations being affected by the natural state of the samples and by laboratory experiments. The majority of volcanic samples contain a mixture of magnetic remanence carriers, which can cause non-ideal behaviour during palaeointensity experiments. Samples may have been oxidised at high or low temperatures in nature, possibly resulting in considerably inaccurate determinations (Tanaka and Kono, 1991; Yamamoto et al., 2003; Tarduno and Smirnov, 2004; Smirnov and Tarduno, 2005; Yamamoto, 2006; Biggin et al., 2007a). In the laboratory, methods that use bulk heating (Thellier and Thellier, 1959; Shaw, 1974) can cause alteration of magnetic minerals, changing the relationship between applied magnetic field and thermoremanent magnetisation (TRM): a common reason for the failure of palaeointensity experiments. Cooling rate differences between nature and the laboratory can also cause over or underestimation of palaeointensity depending upon the dominant remanence carrier (Fox and Aitken, 1980; Halgedahl et al., 1980; Leonhardt et al., 2006). The best method to obtain accurate absolute palaeointensity determinations without ambiguity from non-ideal recorders is still disputed; however, new techniques (Hill and Shaw, 1999; Cottrell and Tarduno,

* Corresponding author at: Institute for Rock Magnetism and Department of Geology and Geophysics, University of Minnesota, Minneapolis, MN 55455, USA.
E-mail addresses: mcbrown@umn.edu, m.c.brown@liv.ac.uk (M.C. Brown).

0031-9201/$ – see front matter.
doi:10.1016/j.pepi.2008.11.001

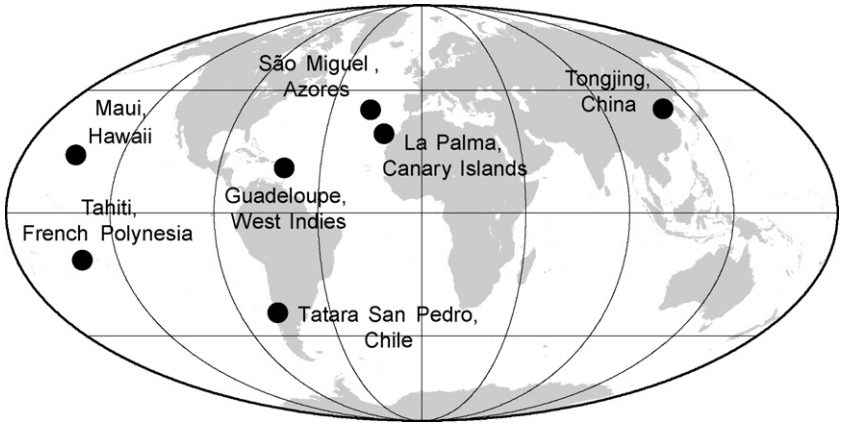

Fig. 1. Location map for lava flows that record the MB reversal. La Palma (Quidelleur and Valet, 1996; Valet et al., 1998, 1999; Quidelleur et al., 1999, 2002, 2003; Singer et al., 2002), Guadeloupe (Carlut et al., 2000; Carlut and Quidelleur, 2000), Tahiti (Chauvin et al., 1990; Mochizuki et al., 2005), Tatara San Pedro (Brown et al., 1994, 2004; Gratton et al., 2007), Maui (Coe et al., 2004), Tongjing (Zhu et al., 1991), São Miguel (Johnson et al., 1998).

1999; Yamamoto et al., 2003; Dekkers and Böhnel, 2006) and new protocols for the Thellier method (Riisager and Riisager, 2001; Fabian, 2001; Yu et al., 2004; Biggin et al., 2007b) have made significant improvements in obtaining accurate data and in detecting data affected by non-ideal remanence carriers.

In addition to having reliable magnetic measurements, accurate dating of both sedimentary and volcanic reversal sequences is required to correlate geomagnetic field variations globally and to constrain the core processes that generate the magnetic field (Singer et al., 2005; Leonhardt and Fabian, 2007). The need for accurate dating is highlighted when the possible complexity and global non-uniformity of the field during a reversal is considered (Coe and Glen, 2004; Brown et al., 2007).

The Matuyama–Brunhes (MB) reversal is the most recent geomagnetic field reversal and is recorded in numerous sedimentary sequences and by 16 volcanic sequences at seven locations globally (Fig. 1). It has also been recorded in the sediments at the Acheulean site of Gesher Benot Ya'aqov, Israel (Verosub et al., 1998; Goren-Inbar et al., 2000). It provides our best chance to characterise a reversal globally.

Astronomical dating, using tuned oxygen isotopes from sediments, places the main polarity change at 781 ± 2 ka in the Atlantic and at 775 ± 2 ka from cores from the Indian-Pacific-Caribbean (Tauxe et al., 1996). A significant reduction in intensity approximately 15 kyr before the main polarity change is also recorded (Hartl and Tauxe, 1996). Astronomical dates from Yamazaki and Oda (2001) from South Atlantic anoxic sediments agree with the 781 ka estimate of Tauxe et al. (1996). They also date a number of large geomagnetic field fluctuations before the main polarity change to be between 788 ka and 795 ka. Channell et al. (2004) using Atlantic sediments south of Iceland have dated the mid-point of the reversal to be between approximately 772.5 ka and 773.5 ka, younger than the mean estimates of previous estimates; however, within the range of results obtained by Tauxe et al. (1996): 769.9 ± 3.8 ka to 784.2 ± 19.4 ka (from 18 sites). The variations in dating could be caused by problems with the sedimentary recording process and/or by real global offsets in the timing of directional changes (Coe et al., 2000; Brown et al., 2007; Leonhardt and Fabian, 2007).

^{40}Ar/ ^{39}Ar dating of lava flows has identified features that may relate to the reversal process or other large fluctuations in the geomagnetic field between 776 ka and 798 ka (Singer et al., 2002; Brown et al., 2004; Coe et al., 2004; Singer et al., 2005). ^{40}K/ ^{40}Ar dating has determined lava flows erupted between approximately 777 ka and 825 ka that again record the MB transition and large variations in the geomagnetic field, which may or may not relate to the reversal process (Valet et al., 1999; Carlut et al., 2000; Carlut and Quidelleur, 2000; Quidelleur et al., 2002, 2003). ^{10}Be records from Antarctic ice cores have also been used to calculate virtual axial dipole moment (VADM) variations at the time of the MB reversal. Raisbeck et al. (2006) calculated two intensity lows, one related to the main polarity change at approximately 780 ka and another at approximately 800 ka.

Global modelling of the MB reversal has been attempted by Shao et al. (1999) and Leonhardt and Fabian (2007) with the IMMAB4 model of Leonhardt and Fabian (2007) being particularly impressive in its approach and its reproducibility of some features of the MB transitional field; however, as the authors note, more detailed palaeomagnetic records of transitional fields are required to gain further insight into the reversal process. We aim to provide new reliable microwave palaeointensity and thermal palaeodirection data for the reversal. In this study we have revisited four sections from the island of La Palma, Canary Islands, and one section from the island of Guadeloupe, West Indies. A recent study of the MB reversal by Gratton et al. (2007) using the microwave palaeointensity technique was able to determine palaeointensity from a series of lava flows from Chile recording the transitional field. This motivated us to re-examine these sections with the hope of improving the palaeointensity record.

2. Background

2.1. La Palma

The island of La Palma in the Canary Archipelago (Fig. 2a and b) is positioned on the slow moving African plate approximately 100 km north of the possible emergence of a mantle plume beneath the island of El Hierro (Prægel and Holm, 2006). Apart from the Hawaiian Islands, the Canary Islands are the most studied group of islands in the world (Carracedo et al., 1998). Unlike other intraplate oceanic islands, such as the Hawaiian-Emperor chain, the Canary Islands are located over very old crust (the crust underlying La Palma and El Hierro being 150–156 Ma; Watts, 1994) and are near a passive continental margin (Carracedo et al., 2007). The archeapelago has developed over the last 30 million years, with the age of the islands increasing from east to west (Carracedo et al., 1998), possibly as a result of the west–east movement of the African plate over a mantle hotspot (Holik et al., 1991; Guillou et al., 2001).

La Palma rises 6500 m above the sea floor and 2400 m above sea level (Valet et al., 1999). La Palma is presently in the shield-stage of growth and is the fast growing island in the archipelago (Carracedo et al., 1999; Guillou et al., 2001). It can be divided into three main geological units (Singer et al., 2002): (1) basement

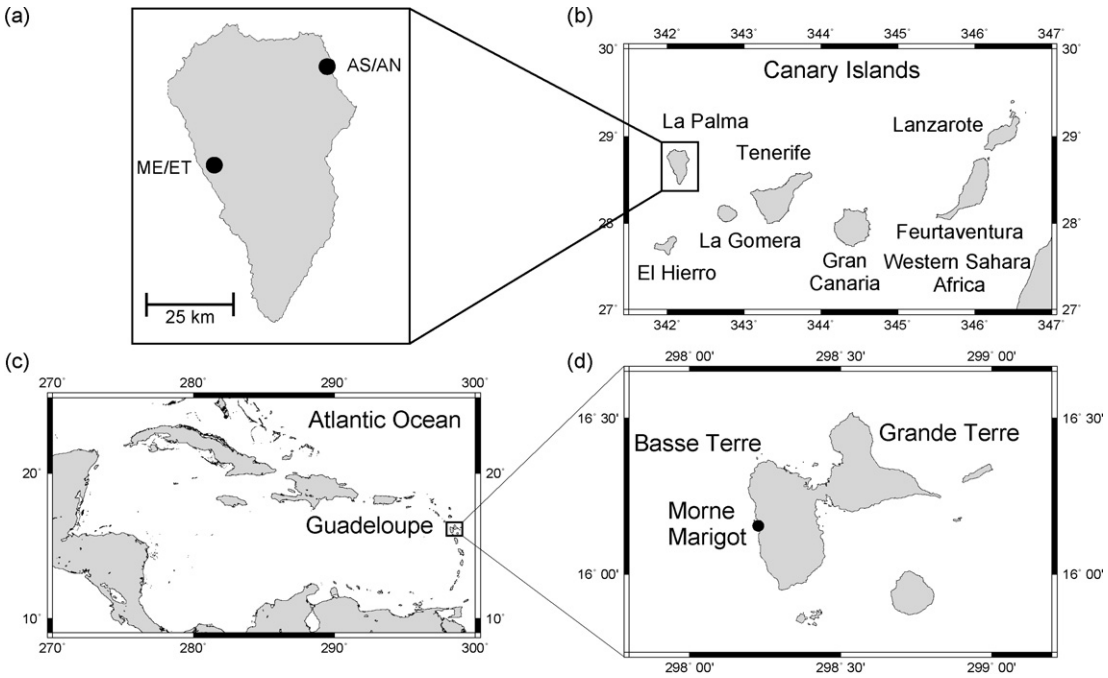

Fig. 2. (a) Map of La Palma with studied sections labelled. (b) La Palma in relation to the other Canary Islands. (c) Guadeloupe's position in the Caribbean island chain. (d) Location of the Morne Marigot quarry sections on the island of Basse Terre, Guadeloupe.

intrusive rocks exposed in the Caldera de Taburiente, which are part of the exhumed Pliocene sea mount; (2) older subaerial lavas which form the Taburiente and Bejenado volcanoes; (3) the younger Cumbre Vieja volcano (Staudigel et al., 1986; Guillou et al., 1998; Carracedo et al., 1999). The Taburiente Volcano formed the north part of the island during the Matuyama and Brunhes chrons, with $^{40}K/^{40}Ar$ and $^{40}Ar/^{39}Ar$ ages dating lavas between 1.6 Ma to 0.5 Ma (Carracedo et al., 1999; Quidelleur et al., 1999, 2002, 2003; Tauxe et al., 2000; Valet et al., 1999; Guillou et al., 2001).

ME and ET sections previously studied by Valet et al. (1998, 1999) are located at El Time in the western part of La Palma (Fig. 2a) and are part of the northwestern flank of the Caldera de Taburiente, which was formed by large landslides (Ancochea et al., 1994). This section either belongs to the Upper Old Series (Ancochea et al., 1994) or the Cumbre Nueva Series (Navarro and Coello, 1993) and therefore could have originated from two different eruptive centres. Palaeosol and cindercone layers are common throughout both sections. The ET section is especially complicated, with flows pinching in and out and intersected by dykes.

Palaeomagnetic sampling was conducted in March 2006. Using previous field notes (VS) and markers left by Valet et al. (1998, 1999) we sampled the same sections and flows as Valet et al. (1999). The ME and ET sections are located at 28.67°N, 17.94°W, approximately 700 m apart along the road LP-1. All flows are approximately horizontal; however, given their thin nature and the distance between the sections, it was not possible to correlate the two sections in the field. We sampled five flows from the ET section and the top 20 flows of the ME section. All cores taken as part of this study were 25 mm in diameter. 11 cores were taken from the ET flows and 100 from the ME flows. We sampled the centres of the flows to avoid problems with remagnetisation by overlying flows (Valet et al., 1998). $^{40}K/^{40}Ar$ dates place from the ME section two flows either side of the polarity reversal at 788 ± 12 ka and 784 ± 13 ka (Quidelleur et al., 2003).

The study of Valet et al. (1999) provides one of the most detailed records on palaeointensity variations around a geomagnetic field reversal. Although no transitional directions were obtained from these sections, palaeointensity was determined from 45 volcanic units. Results varied from 15 μT to 60 μT for a number of flows with stable directions before reducing to ~7 μT prior to the polarity change. Palaeointensity after the reversal was also variable, recovering to ~60 μT. Compared with other intensity data from the PINT03 database (Perrin and Schnepp, 2004) for the last 5 Ma these results seem anomalously high. The palaeointensity records from the ME and ET sections were used to calibrate the relative intensity data from the sedimentary records used in IMMAB4 (Leonhardt and Fabian, 2007).

The AS and AN sections are located in the Barranco del Agua, in the north east of the island (Fig. 2a) (28.80°N, 17.77°W). The lava flows are basaltic and part of the Upper Old Series of the Taburiente Stratovolcano (Navarro and Coello, 1993). It is unclear whether these flows are from the same eruptive centre that produced the flows at El Time. Scoria layers (in one case 5 metres thick) and palaeosols are again seen.

We roughly followed the sampling of Quidelleur and Valet (1996) and Singer et al. (2002) on the southern side of the gorge; the AS section (LL in Quidelleur and Valet, 1996 and TS in Singer et al., 2002). For the northern side of the gorge (AN section) we followed the vertical section chosen by Quidelleur and Valet (1996) (LS section). The TN section from Singer et al. (2002) was difficult to trace and we were not confident that we could resolve an accurate stratigraphy. The large number of flows and ambiguity in the delimitation of some of the flows means that the results from our study and the Quidelleur and Valet (1996) and Singer et al. (2002) studies cannot be directly compared. 77 cores were taken from 20 flows from the AS section that sample the time around the reversal (107 cores from 29 flows were sampled in total; the youngest flows contain an excursion around 600 ka (Quidelleur et al., 1999) or 580 ka (Singer et al., 2002)). 57 cores were taken from 16 flows from the AN section.

Quidelleur and Valet (1996) obtained both palaeodirection and palaeointensity results from flows on both sides of the gorge. Palaeointensity was obtained from 17 flows; however, results from 9 flows were corrected using the method of Valet et al. (1996). Palaeointensity prior to the polarity change is low with a minimum value of 4 μT. One $^{40}K/^{40}Ar$ date of 797 ± 12 ka was obtained

from the northern side of the gorge from a reversed polarity flow (Quidelleur et al., 2002). No transitional directions were obtained in the Quidelleur and Valet (1996) study; however, Singer et al. (2002) sampling a different section on the northern side of the gorge found two flows that recorded transitionally reversed directions. These flows were dated by ^{40}Ar/ ^{39}Ar to be 780 ± 10 ka and 803 ± 10 ka. Two flows lower in the stratigraphy were dated at 791 ± 19 ka and 796 ± 10 ka and Singer et al. (2002, 2005) suggest these flows record a precursor event to the main polarity change of the MB (Hartl and Tauxe, 1996; Brown et al., 2004; Gratton et al., 2007).

2.2. Guadeloupe

The volcanic island of Guadeloupe is situated in the West Indies in the Atlantic Ocean (Fig. 2a) and is part of an island arc resulting from the subduction of the Atlantic plate under the Caribbean plate (Komorowski et al., 2005). The island is divided into two distinct parts; the older Grande-Terre in the east and Basse-Terre to the west. Grande-Terre comprises older volcanics of pre-Miocene age overlain with Pleistocene limestone, while Basse-Terre is entirely volcanic; the oldest parts of the island thought to be no older than 2.79 Ma from ^{40}K/ ^{40}Ar dating methods (Samper et al., 2007).

Palaeomagnetic sampling took place in March 2005 (MCB and MNG) and was concentrated on the southern part of the west coast of Basse Terre (Fig. 2b), where the age of volcanism was determined to be less than 1 Ma by ^{40}K/ ^{40}Ar dating (Blanc, 1983; Carlut et al., 2000, further ^{40}K/ ^{40}Ar dating by Samper et al., 2007 subsequent to our field trip is in agreement with this conclusion). The sampling sites for this study are: (1) Morne Marigot quarry (16.1°N, 298.2°E), at a rare exposure of superposed andesitic lavas (heavy vegetation on the island prevents good rock exposure); (2) a river cut section ∼500 m to the south west of the quarry and ∼20 m below the base of the quarry.

We re-sampled the same Morne Marigot quarry flows studied in Carlut et al. (2000) and Carlut and Quidelleur (2000). Carlut and Quidelleur (2000) first identified field variations related to the MB reversal in sections at Morne Marigot in three flows. Following alternating field and thermal demagnetisation experiments, a change in polarity up the sequence, from transitional to reversed to normal from bottom to top, was observed. ^{40}K/ ^{40}Ar dating of the lava flows yielded dates of 777 ± 14 ka for the stratigraphically lowest (transitional) flow (GU09) and 785 ± 19 ka for the stratigraphically highest (normal) flow (GU11), respectively. These ages identified the sequence as partially recording the MB reversal. Carlut et al. (2000) carried out palaeointensity experiments on these three flows, using the double-heating variant of the Thellier method (Coe, 1967). Some experiments were conducted in an Argon atmosphere, and some heated in air. Four samples yielded a mean flow value of 5.5 ± 1.0 μT for the reversed flow (GU09) and two samples yielded a mean flow value of 11.0 ± 2.7 μT for the normal flow (GU11), with one value corrected for non-linearity in the Arai-Nagata plot, using the correction method of (Valet et al., 1996). The transitional polarity flow (GU10) did not yield any palaeointensities because of thermochemical alteration observed during the Thellier experiments (Carlut et al., 2000). It is the failure of the Thermal palaeointensity experiments that prompted us to try microwave palaeointensity analysis to obtain transitional palaeointensity data from this section.

In this study we have called flows GU09, GU10 and GU11 from Carlut et al. (2000) and Carlut and Quidelleur (2000) G01, G02 and G03 and divided the quarry into three vertical sections: A, B and C. Vertical sections were approximately 55 m apart. The A section included all three flows; B included G01 and G02; C only sampled G01. The quarry was heavily vegetated so exposure was limited. G01 is the lowest stratigraphic unit of these three and is 160 m in lateral extent, with an average flow thickness of 7 m with 4 m of scoria on top; G02 is 10 m thick on average with 3 m of scoria above that; G03 is the highest stratigraphic unit and is on average 3 m thick with 3 m of scoria above that. 20 cores were sampled from G01, 14 were sampled from G02 and 8 were sampled from G03. Cores were taken in vertical sections throughout the thickness of the flows, with sample 01 being near to base of the exposed flow.

The river cut section is labelled GD and has not been sampled before. No radiometric dates exist; however, the height of the flow and the roughly horizontal dip of the flows in this area suggests that GD is older than the sequence at Morne Marigot. It was sampled to provide directional and palaeointensity information prior to the transitional sequence. 8 cores were sampled.

The La Palma flows are labelled in ascending number order from oldest to youngest and also given a flow number (FN). All graphs showing results from individual flows are plotted as flow number. For the Guadeloupe flows we have retained the names assigned in the field and we have again given the flows a flow number. Conversions of the Guadeloupe field names to the flow numbers are shown in Table A.4.

3. Methods

3.1. Rock magnetic methods

A number of magnetic property measurements were made on samples from the La Palma and Guadeloupe sections to evaluate their suitability for palaeointensity experiments and to identify those samples which might be expected to give the most accurate results. Multiple measurements were made on 5 mm sub-samples from 25 mm cores and from multiple 25 mm cores per flows. Hysteresis and back field coercivity measurements were carried out on a Variable Field Translation Balance (MMVFTB) at the University of Liverpool and on a Princeton Measurement Corporation Micro-Mag 2900 vibrating sample magnetometer (VSM) at the Institute for Rock Magnetism, University of Minnesota. Hysteresis measurements allow the determination of saturation magnetisation, M_s, saturation of remanence, M_{rs}, and coercivity, H_c; back field remanence measurements give H_{cr}. These measurements have been used to calculate ratios of M_{rs}/M_s and H_{cr}/H_c and plotted as a Day plot (Day et al., 1977) or a squareness plot (Tauxe et al., 2002).

Thermomagnetic measurements were carried out in air using the MMVFTB. Magnetisation in an applied field of 0.75 T was measured as temperature was increased from room temperature to 700 ° C and then allowed to cool back to room temperature. All thermomagnetic curves are corrected for their paramagnetic content, calculated from hysteresis measurements on the same sample prior to heating using the VFTB. Curie temperature is determined using the extrapolation method (Moskowitz, 1981). The titanium content of the titanomagnetite is estimated using a polynomial fit to experimental data for synthetic titanomagnetites (Bleil and Petersen, 1982). We recognise the limitations of this approach for determining the composition of natural titanomagnetites (see Lattard et al., 2006).

Low temperature susceptibility was measured on a small number of samples from the ME section using a Quantum Design Magnetic Properties Measurement System at the Institute for Rock Magnetism, University of Minnesota. Temperature was increased from 5 K to 300 K and measured at 1 Hz. Multiple samples per flow were measured on a Bartington MS2 susceptibility meter at the Geomagnetism Laboratory, University of Liverpool. 1 mm × 5 mm discs of the cores were placed in liquid nitrogen for 20 min and then allowed to heat up in the ambient conditions of the laboratory while susceptibility was continuously measured.

3.2. Thermal demagnetisation

Thermal demagnetisation was used to obtain palaeodirections from samples from La Palma and Guadeloupe. A Magnetic Measurements thermal demagnetiser was used to demagnetise the samples and magnetic measurements were made using a Molspin spinner magnetometer. Samples were demagnetised in 50° C steps up to 500° C and then in 20° C steps until the remanent magnetisation was lost (typically around 540 °C). Multiple 25 mm samples per flow were used to determine the directional changes recorded in the AS, AN and Guadeloupe sections (see tables in Appendix A). Only one sample per flow was used for the ME section as our initial results were in agreement with those obtained by Valet et al. (1999). Flows from the ET section appeared very weathered when sampled in the field and pilot microwave demagnetisation experiments revealed multiple components of magnetisation. These samples are not suitable for directional or palaeointensity analysis and no further experiments were performed on samples from this section.

3.3. Microwave palaeointensity method

The microwave method is an alternative to thermal techniques and can substantially limit thermochemical alteration of magnetic grains during experimentation; such alteration is the main reason for the failure of palaeointensity experiments with thermal techniques such as the Thellier (Thellier and Thellier, 1959; Coe, 1967) and Shaw techniques (Shaw, 1974; Rolph and Shaw, 1985). Thermal methods involve bulk heating samples, creating phonons (lattice vibrations) that then generate magnons (electron spin waves) causing the magnetic grains to demagnetise in a zero field. The microwave procedure does not use bulk heating of the sample matrix, but instead uses high-frequency microwaves that are resonant with the magnetic grains, exciting the magnons within those grains directly (Walton, 2002, 2004a, b; Walton et al., 2004). It has been shown by Hill et al. (2002a) and Biggin et al. (2007b) that in most cases were both methods are successful microwave-thermoremanent magnetisation (T_MRM) is equivalent to conventional thermoremanent magnetisation (TRM).

From January 2007, two 14 GHz microwave systems with 80 W amplifiers have been in operation at the Geomagnetism Laboratory, University of Liverpool: one with a liquid-nitrogen FIT SQUID magnetometer and another with a more sensitive three axis liquid-helium Tristan Technologies SQUID magnetometer (maximum sensitivity $\sim 1 \times 10^{-11}$ A m^2; Shaw and Share, 2007). The systems have different microwave resonant cavities. Both systems have programmable field coils (up to 100 μT) surrounding the microwave cavity and a T_MRM can be induced in any specified direction. This allowed us to address whether there was any biasing of palaeointensity determinations caused by a particular experimental methodology. Three different protocols were used: the perpendicular method (Kono and Ueno, 1977; Hill and Shaw, 2007), the double-heating method (Coe, 1967) and the quasi-perpendicular method (Biggin et al., 2007b). The majority of experiments used the perpendicular method. The microwave system with the Tristan magnetometer was only used for the quasi-perpendicular experiments.

5 mm samples were drilled from 25 mm cores and were attached by glue to the sample rod. During the experiments microwave power was applied for 5 s for each step. Microwave power was increased in steps at the discretion of the operator; the next step was determined based on the result of the previous step. Once the maximum power of 80 W was reached, the time of microwave power application was increased until a maximum of 20 s and the experiment stopped when the sample was fully demagnetised or became detached from the sample rod. After each measurement declination and inclination are calculated and outputted by the control computer. This is of great importance when using the perpendicular protocol as the primary component of magnetisation must be used when determining a palaeointensity by this method. This, therefore, allows us to know when we have isolated the primary component of magnetisation. Further experimental details and the development of the systems are well documented in Hill et al. (2002a, b, 2005), McArdle et al. (2004) and Gratton et al. (2005a, b, 2007).

3.4. Palaeointensity acceptability criteria

Palaeointensity estimates have been accessed using the criteria of Brown et al. (2006) and are split in to three categories: class 1, class 2, and class 3. Three classes were chosen as they more successfully represent the variation in the quality of the data in this study. A class 1 result must have the following:

(1) A stable primary natural remanent magnetisation (NRM) direction.
(2) Greater than or equal to four data points in a single straight line on an NRM/T_MRM plot. No point is eliminated in the selected NRM segment, unless it can be proved to be caused by experimental error (these results are shown in open circles).
(3) At least 30defined by Coe et al., 1978).
(4) A quality factor, q (defined in Coe et al., 1978) ≥ 5.
(5) A gap factor, g (defined in Coe et al., 1978) > 0.5.
(6) A regression coefficient, r^2 of the best-fitting line ≥ 0.98.
(7) For determinations made using the perpendicular method, $\theta_1 + \theta_2$ must be between 90° and 91° (the sum of the angles between the NRM and the (T_MRM) vector and the applied field vector and the (T_MRM) vector; Hill and Shaw, 2007).
(8) pT_MRM checks differing from the original value by $\leq$ 10% (using the DRAT criteria of Selkin and Tauxe, 2000).
(9) pT_MRM $\leq$ 10% difference between two zero field applied power steps ($P_i - P_{i-1}$, where P_i is a given applied microwave power Riisager and Riisager, 2001) for double-heating experiments.

A class 2 result must pass all the criteria listed; however, it may fail pT_MRM checks or pT_MRM tail checks if there is little or no distortion to the straight line trend. This suggests that the check failure is caused by problems with the reproducibility of the reflected power in the microwave cavity during the microwave experiment rather than by alteration or non-ideal behaviour. This category has been included as many of the results have high f, q and r^2 values but display this kind of behaviour. Results from the quasi-perpendicular method are class 2. Although this protocol has been successful in determining the historical geomagnetic field from lavas with a range of magnetic domain states where other protocols failed (Biggin et al., 2007a, b), it requires further validation. Class 3 results produce a linear relationship between NRM and T_MRM ($r^2 \geq 0.9$) but fail some of the selection criteria and checks, and represent data that are unreliable.

4. Results

4.1. Rock magnetism

4.1.1. La Palma

Hysteresis parameters are plotted in Fig. 3a and c. The majority of samples plot in the pseudo-single domain (PSD) area of the Day et al. (1977) plot and along the theoretical mixing curves of single domain (SD) and multi-domain (MD) particles for TM0 from Dunlop (2002a, b). All La Palma flows have similar characteristics on the Day et al. (1977) plot and squareness against coercivity plots (Tauxe et al., 2002). All flows show a spread in M_{rs}/M_s, H_c and H_{cr}/H_c to some degree. Some flows show a spread in H_{cr}/H_c up to 4 and in M_{rs}/M_s

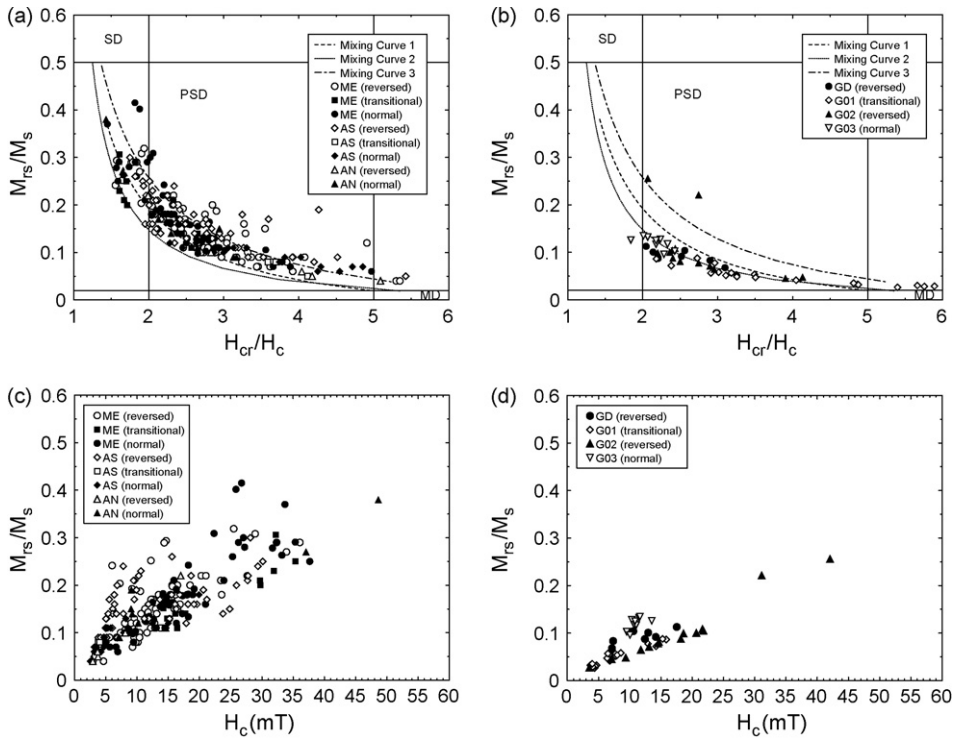

Fig. 3. Day et al. (1977) plots (a and b) and squareness against coercivity plots (Tauxe et al., 2002), (c and d) for La Palma (a and c) and Guadeloupe (b and d) lava flows. Samples split between reversed, transitional and normal field directions. Transitional flows are ME45, ME46 and AS14. Day et al. (1977) plots modified using results from (Dunlop, 2002a, b). Curves 1–3 are theoretical mixing curves of SD and MD particles for TM0 from Dunlop (2002a, b).

up to 0.3 (e.g. ME49). In these cases there is a range of magnetic particle types and behaviour.

Three broad types of thermomagnetic behaviour have been identified for the La Palma samples: types 1, 3 and 5 (Fig. 4). 171 samples from all La Palma sections were measured. 63 samples from 33 flows show type 1 behaviour. Type 1 curves show a single magnetic phase with Curie temperatures between 446 ° C and 540 °C, corresponding to possible titanomagnetite compositions between TM19 and TM07. Magnetisation is reduced on cooling and there is range of irreversibility. At 100 ° C the difference in induced magnetisation between the two curves ranges from 3% to 45%. The magnetic phase producing type 1 behaviour could either be a low Ti-titanomagnetite or may result from high temperature deuteric oxidation of primary high titanium titanomagnetite producing a low titanium titanomagnetite phase (Carmichael and Nicolls, 1967; Mankinen et al., 1985). No microscopy was carried out as part of the present study, so oxidation cannot be confirmed.

Type 3 curves (Fig. 4c–e) (70 samples from 45 flows) have a low titanium titanomagnetite phase (Curie temperatures between 398 ° C and 580 °C, corresponding to compositions between TM29 and TM0) and another higher titanium titanomagnetite phase (Curie temperatures between 131 ° C and 333 °C, corresponding to compositions between TM67 and TM38). The three divisions of type 3 show the variations in the titanomagnetite compositions. Such heating curves have been previously been observed for samples where high temperature deuteric oxidation has converted only part of the high titanium titanomagnetite phase to a low titanium titanomagnetite phase or the low Curie temperature phase results from the presence of titanomaghemite. All type 3 cooling curves show an increase in induced magnetisation (at least for some of the temperature range (type 3a)). Type 3c curves show the largest increase in induced magnetisation (up to 66% at 100 °C). Some cooling curves show complete oxidation of the high titanium titanomagnetite phase to a single lower titanium phase (Fig. 4c). Other cooling curves show less oxidation of the higher titanium phase (Fig. 4d and e).

Type 5a and 5b curves (Fig. 4g and h) (39 samples from 18 flows) show a range of low Curie temperatures from between 94 ° C and 143 °C. On heating, Curie temperatures rise to between approximately 450 ° C and 550 ° C and the curves show pronounced irreversibility. In some examples there is an increase in induced magnetisation on cooling (measured at 100 °C) up to 14 times the original magnetisation. The oxidation product at the higher Curie temperature could either be titanomaghemite or a low titanium titanomagnetite formed from a primary high titanium titanomagnetite (between TM71 and TM65). In type 5a curves there is a very slight increase in induced magnetisation between 400 ° C and 500 ° C which could suggest inversion of titanomaghemite to titanomagnetite; however, without performing thermomagnetic experiments in a vacuum it is not possible to determine whether this bump and the large increase in induced magnetisation on cooling are a product of oxidation during the laboratory heating or to the inversion of titanomaghemite to titanomagnetite. Type 5b curves do not show an increase in induced magnetisation on heating between 400 ° C and 500 °C. On cooling, type 5a curves show a mixture of secondary magnetic phases, whereas type 5b curves show a single secondary magnetic phase. An example of a microwave palaeointensity experiment performed on a sample with type 5b behaviour is shown in Fig. 11c.

Type 1 curves were dominant for the ME section (41 samples from 25 flows) and there were no examples of type 5 curves. The AS section was approximately equally divided between type 1, type 3 and type 5 curves. Type 3 curves were dominant for the AN section (11 samples from 11 flows). For a number of flows the thermomagnetic behaviour within a type is variable and for a number of flows two types of curve have been observed. For example, AS10 shows both type 1 and type 5 curves. This variation could result from inhomogeneous starting compositions or to inhomogeneous oxidation of the titanomagnetite particles during initial

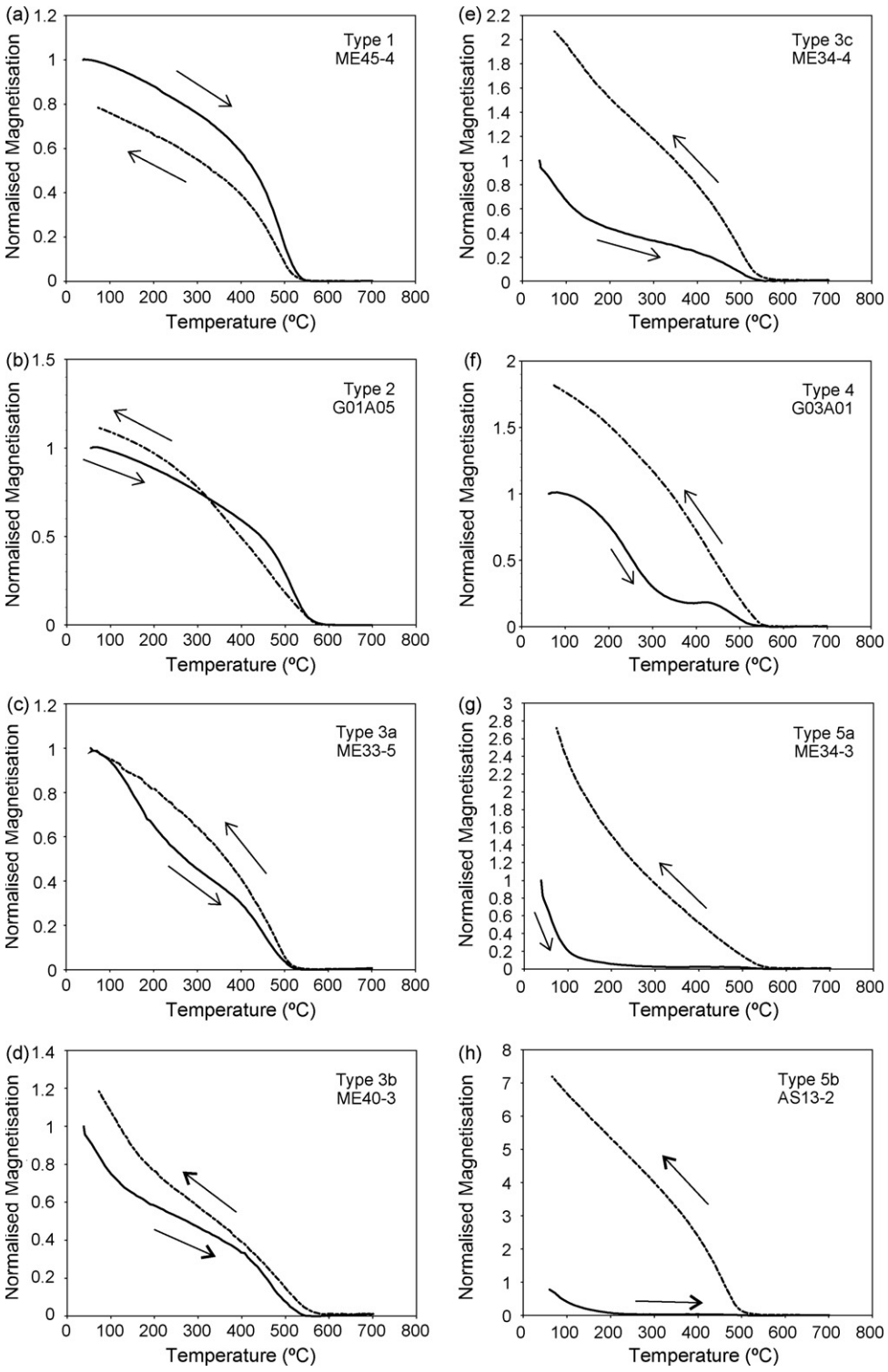

Fig. 4. Examples of the five broad types of thermomagnetic curves from samples from La Palma and Guadeloupe. Arrows indicate heating (solid lines) and cooling (dashed lines).

cooling at high temperature or by low temperature oxidation during weathering.

Examples of low-temperature susceptibility curves are shown in Fig. 5. 210 samples were tested and a range of low-temperature behaviour was determined. They are broadly categorised into four types (Fig. 5a–d). Considering titanomagnetite as the dominant magnetic phase in this sample set, low-temperature behaviour is influenced by a number factors including composition (titanium content in titanomagnetite; Moskowitz et al., 1998) and oxidation (either partial maghemitisation of magnetite at low temperatures (Özdemir et al., 1993) or to possible homogenisation of ilmenite intergrowths to titanomagnetite at high temperatures; cf. Smirnov and Tarduno, 2005). Fig. 5a shows a susceptibility maximum at around 85 K. This is probably caused by partial suppression of the Verwey transition of a low titanium titanomagnetite phase containing MD particles (Moskowitz, 1981) and could be caused by a

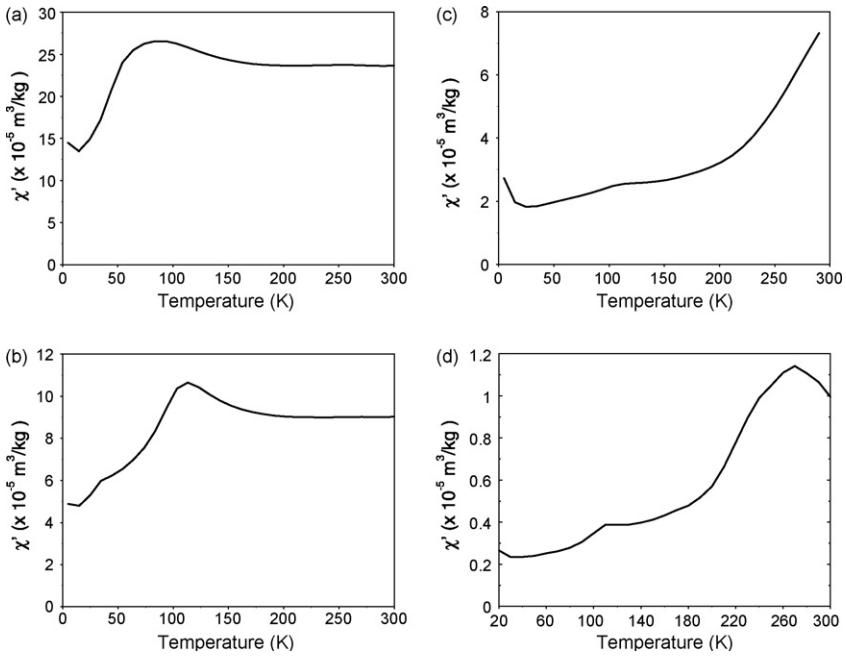

Fig. 5. Examples of low temperature frequency dependence of susceptibility measurements for the ME section, La Palma. Samples shown are (a) ME32-1A1; (b) ME47-2A; (c) ME36-1A1; (d) ME41-3B.

degree of partial oxidation. In some examples the transition is very suppressed with the ratio of initial susceptibility to room temperature susceptibility exceeding 1 and a disappearance of any isotropic point. In Fig. 4b there is an inflection at around 50 K and a susceptibility peak between 100 K and 120 K. The former could be caused by the presence of an ilmenite phase (Yamamoto, 2006). The latter could be caused by the presence of titanium poor titanomagnetite of varying compositions. These observations are consistent with the results of the thermomagnetic experiments: Fig. 5a and b are both from samples which show type 1 thermomagnetic heating and cooling curves (they suggest the existence of low-Ti titanomagnetite without any indication of low-temperature oxidation). In Fig. 4c and d there are inflection points around 110 K, although they are not as pronounced compared with those shown in Fig. 4a and b. These curves were observed from samples showing both type 1 and type 3 thermomagnetic heating and cooling curves suggesting that no low-temperature oxidation is present. Therefore, the inflection points probably originate from the Verwey transition of low-Ti titanomagnetite. Many flows show an internal variation of low temperature susceptibility characteristics and this in agreement with the high temperature heating and cooling curves. Such variation could possibly represent inhomogeneous deuteric oxidation of the flows.

4.1.2. Guadeloupe

Hysteresis parameters are shown in Fig. 3b and d. Each flow has a distinctive distribution, but this does not relate to the palaeomagnetic direction recorded by the flow. The Day et al. (1977) plot shows that G01 (the transitional flow) has a range of particle types, but many samples are dominated by MD particles. G02 shows the biggest spread in hysteresis parameters, whereas G03 shows a tight cluster on both the Day et al. (1977) plot and the squareness against coercivity plots.

Four types of thermomagnetic curves are observed for the four Guadeloupe flows: types 1, 2, 3 and 4 (Fig. 4). Type 1 curves (Fig. 4a) were determined from 29 samples from GD, G01 and G02. Curie temperatures range from 522 °C to 580 °C corresponding to compositions from TM09 to TM0. Induced magnetisation was reduced on cooling and the curves showed a range of irreversibility from 0% to 92% difference in induced magnetisation at 100 °C. Seven type 1 curves show a small contribution from a second higher titanium titanomagnetite phase on heating above 500 °C. In some examples this phase has a Curie temperature close to the primary phase. On cooling, a single phase was formed, with a lower Curie temperature and a reduction in induced magnetisation across the whole temperature range.

Type 2 curves (Fig. 4b) show a single phase, a small secondary phase or a mixture of phases on heating. On cooling the heating and cooling curves cross. 11 samples from all four flows show this behaviour. Some examples have a reduced Curie temperature on cooling and some have the same or slightly higher Curie temperature as the primary phase. This behaviour could result from a combination of oxidation of the low titanium titanomagnetite and alteration of the higher titanium magnetite to a lower titanium phase on heating. Type 3 curves were only observed for 10 samples from G01 and G03.

Type 4 curves (Fig. 4f) show a distinctive inflection point at around 420 °C. Before this inflection there is a small increase induced magnetisation between 400 ° C and 420 °C. This behaviour indicates un-mixing and inversion of titanomaghemitite to titanomagnetite (Moskowitz, 1981). In these examples the amount of low-temperature oxidation of the primary titanomagnetite to titanomaghemite is thought to be low (Yamamoto and Tsunakawa, 2005). Only four samples from GA03 showed this behaviour; however, it could suggest that type 4 samples from GA03 contain a mixture of titanomaghemite and titanomagnetite phases. Samples showing evidence of maghemitisation will be unsuitable for accurate palaeointensity determinations as their NRM will be a mixture of a TRM, and a chemical remanent magnetisation (CRM) carried by titanomaghemite (Tarduno and Smirnov, 2004). There are variations in thermomagnetic properties within the flows which could again suggest inhomogeneous oxidation of the lava flows and the magnetic minerals.

47 samples from the four flows underwent low-temperature susceptibility measurements. Like the samples from La Palma, Guadeloupe samples show a range of low-temperature curves, and also show large internal variations. This could again be interpreted as showing varying degrees of deuteric oxidation.

4.2. Directional results

From the ME section, La Palma, a 25 mm core from each of the 17 flows sampled was thermally demagnetised. The results are shown in Table A.1 and Fig. 6. 15 cores gave reliable directions that are in good agreement with the results from Valet et al. (1999). All samples record a secondary component of magnetisation, which was removed between 350° C and 400° C (Fig. 7). (This component was also removed before applying the field in the perpendicular microwave palaeointensity experiment.) All samples that are accepted record vectors with maximum angular deviation (M.A.D.) (Kirschvink, 1980) less than 10°. 12 samples have M.A.D. less than 5°. The two flows that give no results are ME45 and ME46. These flows were emplaced between two flows recording reversed and normal directions and show overlapping components of magnetisation with high un-blocking temperatures, without a clear high temperature characteristic remanence component (Fig. 7b). These flows were studied in detail by Valet et al. (1998) and they concluded that the complexity of the vector is caused by partial reheating by the overlying flows recording the post-transitional field and by progressive oxidation of titanomagnetite, which raised the Curie temperature of the magnetic grains carrying the remagnetisation (an observation consistent with our thermomagnetic analysis). It has therefore not been possible to obtain either palaeodirections or palaeointensity during the polarity transition.

75 samples from 20 flows from the AS section, La Palma, were thermally demagnetised. A primary component of magnetisation was obtained for 16 flows; however, only 13 flow means were determined from three or more samples per flow. The majority of flows record secondary components of magnetisation, which were removed between 250° C and 400° C (Fig. 7 and Table A.2). We include all 16 flows in our subsequent analysis, but advise great caution when interpreting results from the three flow means determined from less than three directions. All results are shown in Table A.2 and Fig. 6. There is a range of precision in the flow mean directions; from $\alpha_{95} = 1.3$ to $\alpha_{95} = 14.8$. Two flows (AS10 and AS9) have $\alpha_{95} < 5$ and one flow (AS17) has $\alpha_{95} > 10$, the other 10 flows have $5 > \alpha_{95} < 10$. 10 flows record the reversed field, four flows record the normal field and two flows record the transitional field. The precision of the first transitional direction (AS7) is fair (Butler, 1992)($n = 4$, $\alpha_{95} = 9.4$); however, the second transitional direction (AS14) (Fig. 7d) is only determined from one sample (Fig. 7d). The transitional direction determined from AS7 records a large fluctuation (or excursion) in the geomagnetic field before the main polarity change. The timing of this event and how it relates to the evolution of the geomagnetic field is discussed in Section 5.1. Flow AS14 is between a normally and reversely magnetised flow and could record a transitional direction from the main directional reversal.

From the AN section, La Palma, 55 samples from 16 flows were thermally demagnetised. Palaeodirections are obtained for all the flows; however, only eight flow means are determined from three or more samples. 6 flows record large secondary components of magnetisation that were removed between 350° C and 400° C (e.g. Fig. 7g). The other flows record a small viscous component of magnetisation (Fig. 7i). Only three flow mean directions have $\alpha_{95} < 5$,

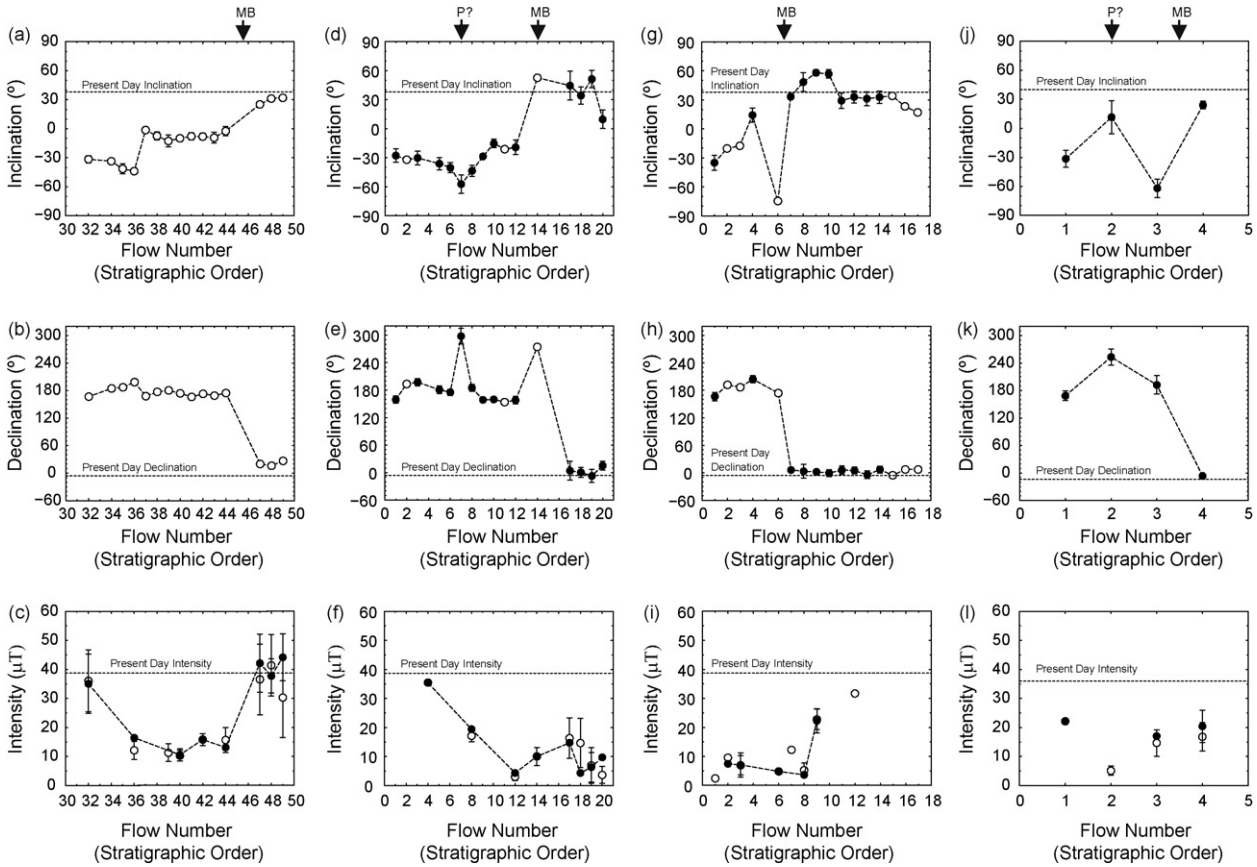

Fig. 6. Inclination, declination and palaeointensity for the ME (a–c), AS (d–f), AN (g–i) and Guadeloupe (j–l) sections. Error bars on ME inclination and declination data are M.A.D. (Kirschvink, 1980) as only one measurement made per flow (see text for details); error bars on AS, AN, and Guadeloupe inclinations are α_{95} (Fisher, 1953) and for the declinations are $\alpha_{95}/\cos(I)$. Directional results: closed circles are flow means calculated from three or more samples; open circles are flow means calculated from less than three samples. Palaeointensity results: solid circles are more robust determinations and are calculated from 1st and 2nd class data (discussed in Section 3.4); open circles are flow mean palaeointensities determined using all estimates presented in Tables B.1–B.3. The dashed lines join flow means calculated using 1st and 2nd class data. MB indicates position of the Matuyama–Brunhes boundary; P? indicates possible position of the precursor or another large fluctuation in the geomagnetic field.

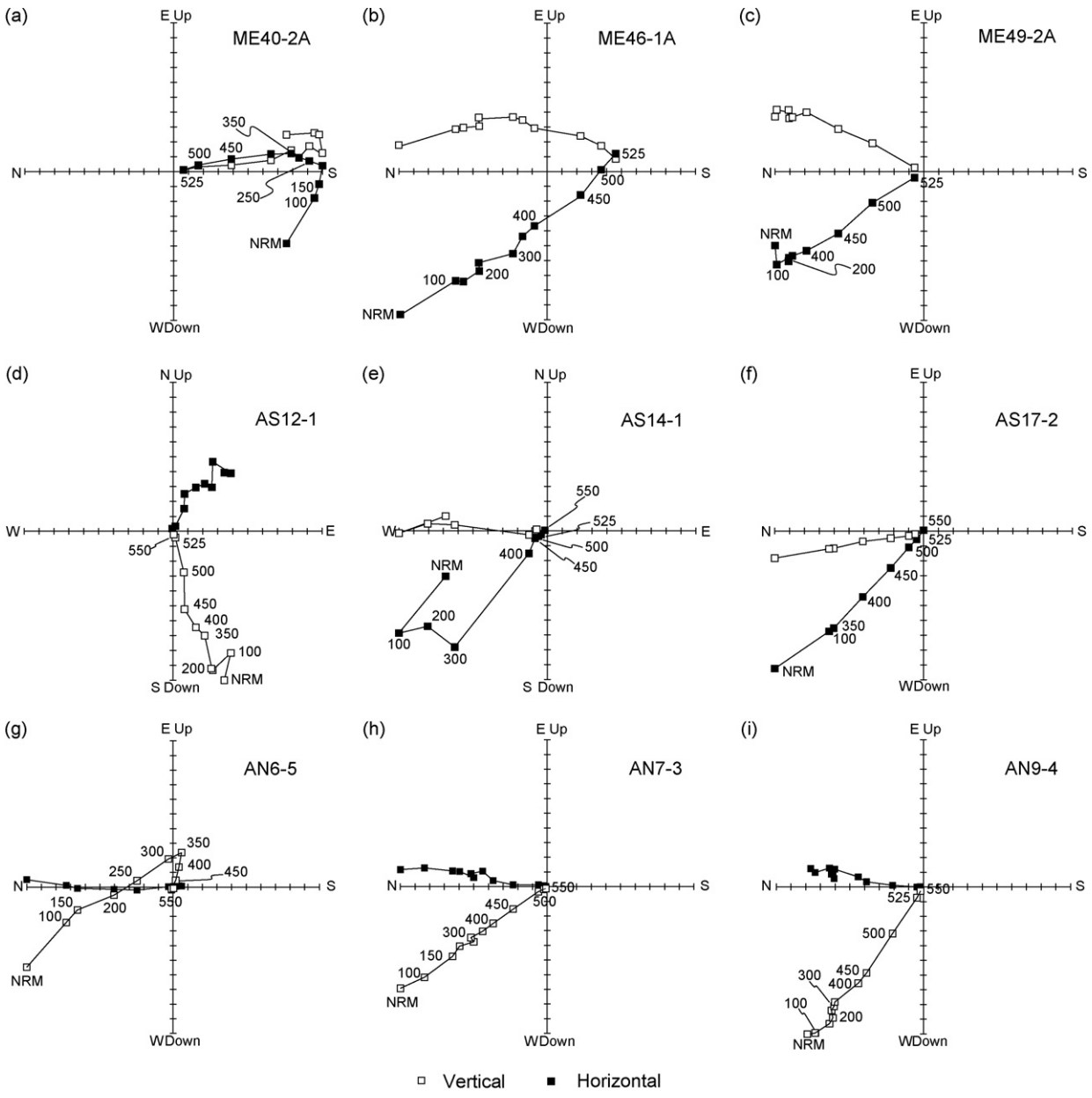

Fig. 7. Examples of orthogonal vector plots from the ME (a–c), AS (d–f) and AN (g–i) sections, La Palma. Plots (a), (d), and (g) show examples from reversely magnetised lavas; (b) and (e) are from transitional magnetised lavas; (c), (f), (h) and (i) are from normally magnetised lavas. (g) and (h) are from lavas that record either side of the MB boundary. Numbers accompanying symbols are temperature in °C.

the remaining five flows have $5 < \alpha_{95} < 10$. All results are shown in Table A.3 and Fig. 6. We again include all 16 determinations in our analysis. No transitional directions were recorded: 5 flows record reversed directions and 11 flows record normal directions. As the normal flows are not dated we do not know if they relate to the reversal process or to more stable field behaviour in the Brunhes chron.

From the Guadeloupe section 26 samples from four flows were thermally demagnetised and 22 samples give reliable directions with an isolated primary component of magnetisation (Table A.4 and Fig. 8). Four samples are rejected because no stable component of magnetisation was recorded or the samples gave significantly different directional results from the majority of other samples in the flow. Samples from G01 (FN2) and G02 (FN3) record large secondary components of magnetisation; however, they were removed between 250 ° C and 300 ° C (Fig. 8). All mean directional results are shown in Table A.4 and Fig. 6. For the stratigraphically lowest flow (GD (FN1)) all seven samples tested record stable primary components of magnetisation, with a mean reversed direction of 169° in declination and −31° in inclination. For flow G01 (FN2), four out of six samples give stable directions, with a mean intermediate polarity direction of 253° in declination and 12° in inclination; however, $\alpha_{95} = 17.1°$. Seven out of eight samples from flow G02 (FN3) again record a reversed stable NRM direction, with a mean value of 192° in declination and −62° in inclination. Flow G03 recorded the most consistent directions ($\alpha_{95} = 3.8$), with four out of five samples giving a stable normal polarity direction: mean declination of 354° and mean inclination of 24°.

4.3. Palaeointensity results

Individual palaeointensity results from the La Palma sections are listed in Tables B.1–B.3. Representative Arai-Nagata plots (Nagata et al., 1963) for class 1 and class 2 data are shown in Fig. 10a–f.

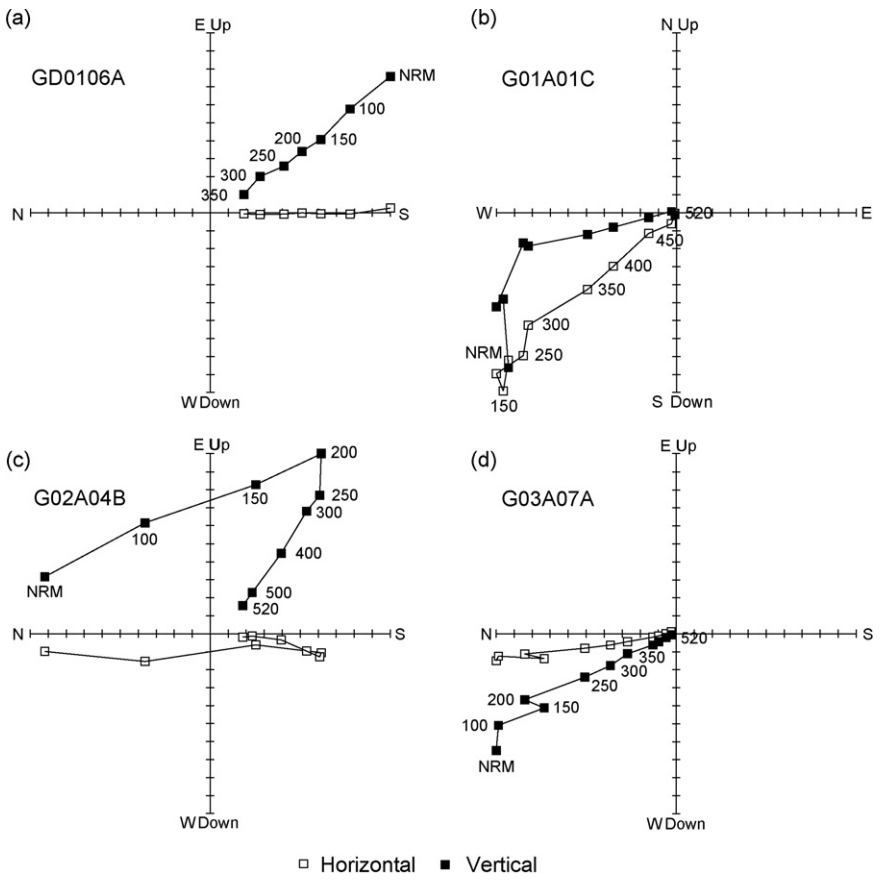

Fig. 8. Examples of orthogonal vector plots from each of the Guadeloupe flows. Numbers accompanying symbols are temperature in °C.

There is a large range in the quality of the palaeointensity results from all sections (Fig. 9) and this can be attributed to the variation in suitability of the samples for palaeointensity experiments. 186 palaeointensity experiments were performed on samples from the ME, AS and AN sections. 119 (64%) experiments produced results that could be classified (classes 1–3); 67 (36%) results are class 1 or 2; 7 (4%) are class 1 (Fig. 9). Palaeointensity results from Guadeloupe are of a lower quality (Fig. 9). From 42 experiments, 19 palaeointensities were determined. Individual palaeointensity results are shown in Table B.4 and in Fig. 10g and h. None passed the class 1 selection criteria and only seven were classified as class 2. The remaining eleven are class 3 results and are likely to be unreliable.

Failure of experiments can be classified into three types:

(1) Apparent instability in the NRM direction. Using the perpendicular method this is detectable by measuring the angle between the characteristic remanence (ChRM) and the resultant vector θ_1, and the angle between the resultant vector and the applied field θ_2 (if the instability is outside the ChRM applied field plane). Variations in $\theta_1 + \theta_2$ can also be generated if the sample is anisotropic, if there is an error in the direction of the applied field, or if the magnetometer is not measuring correctly (Hill and Shaw, 2007). If the NRM directional instability is in the ChRM applied field plane then the relationship between the NRM and T_MRM will be non-linear.
(2) Concave-down NRM T_MRM slopes (Fig. 11a). 23 samples failed because of this behaviour and it was only seen in experiments using the perpendicular method. In all but two examples $\theta_1 + \theta_2$ are between 90° and 91°. There is no apparent relationship between this behaviour and the behaviour of either the pT_MRM checks or T_MRM tail checks; for some points these checks will pass and for others they will fail. A more subtle variant of this behaviour is observed in the quasi-perpendicular experiments. For large fractions of the NRM the relationship between NRM and T_MRM is linear; however, at higher microwave powers a concave-down decreasing slope begins (Fig. 11b). A palaeointensity estimate has been taken for the straight line segment, but this behaviour needs further consideration.
(3) Concave-up NRM T_MRM slopes (Fig. 11c). This behaviour is seen in 11 samples using the double heating or quasi-perpendicular protocol. Four experiments fail pT_MRM checks at maximum microwave power for times greater than 5 s, which would suggest magnetomineralogical alteration. (In theory a small sample in the centre of the cavity will not be subject to high electric fields but in practice this is not true. Magnetic and electric field distribution inside the cavity is influenced by the coupling slot, the sample rod, and the sample. Applying power to a pure quartz sample at 14.2 GHz will eventually heat it, clearly demonstrating the effect of dielectric heating and the presence of alternating electric fields in the sample.) Other examples pass both pT_MRM checks and pT_MRM tail checks, though as in the example shown in Fig. 11c there is failure of some checks.

Flow mean palaeointensities have been calculated in three ways and are shown in Table 1 and plotted in Fig. 6. Using all the data that could be classified, 29 flow means were calculated. The second approach was just only include individual palaeointensity estimates that are class 1 and 2. 25 flow means were calculated from these determinations; however, only 10 of these flows had three or more determinations.

Applying the in-flow variation criterion of Selkin and Tauxe (2000) (the ratio of the standard deviation of the palaeointensity

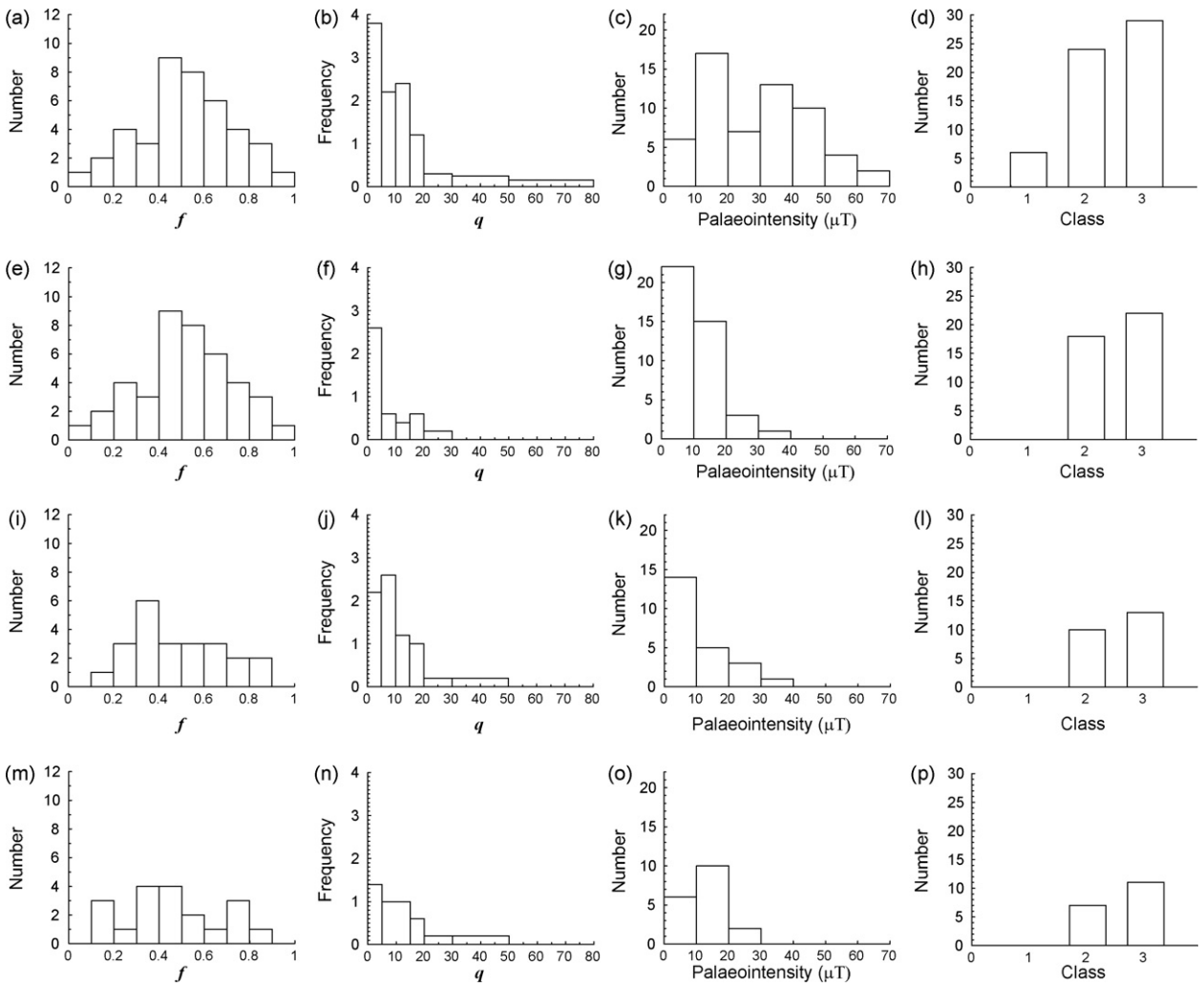

Fig. 9. Bar charts and histograms summarising the quality and number of palaeointensity results. (a–d) Results from the ME section; (e–h) are from the AS section; (i–l) are from the AN section; (m–p) are from the Guadeloupe section. (a, e, i, m) Show the number of results that fall in 0.1 bins of *f* (Coe et al., 1978); (b, f, j, n) show the frequency of results for different intervals of *q* (Coe et al., 1978); (c, g, k, o) show the number of palaeointensity results in 10 μT bins; (d, h, l, p) are the number of results for each class of palaeointensity result, as discussed in Section 3.4

estimates to the mean should be less than 25%) to the flow means calculated from classes 1 and 2 data would cause rejection of a large amount of data with low flow means. For flows with palaeointensity estimates below 10 μT small variations in the estimates can greatly affect the in-flow variation value; this criterion has not been applied to these flows and these results are reliable (Hill et al., 2005). Four flows from the ME section (ME32, ME47, ME48 and ME49) show a large range of palaeointensity determinations. ME32 has an in-flow variation value of 29% and fails the criterion. The three other flows pass the criterion; however, they show non-ideal characteristics for acquisition of thermal remanent magnetisation and for Thellier type palaeointensity determinations. We include these four flows in the further analysis, but express caution over their reliability.

5. Discussion

We discuss the temporal and global evolution of the field during the MB reversal and compare our data with previously published data. We also compare our results with the output generated by model IMMAB4 by Leonhardt and Fabian (2007) and a simple mathematical reversal model (Brown et al., 2007) based upon CALS7K.2 (Korte and Constable, 2005). Even though our data set is small, it is possible to make direct comparisons to IMMAB4; however, only a statistical comparison can be made to the model based on CALS7K.2.

IMMAB4 is global geomagnetic field model of the MB reversal and uses an iterative Bayesian inversion method to construct a spherical harmonic expansion of the transitional field from paleomagnetic data. The initial model is based on the Atlantic ODP core of Valet et al. (1989) with the second iteration including a calibration for absolute palaeointensity from the volcanic section ME-ET, La Palma, from Valet et al. (1999). Subsequent iterations include the Atlantic sedimentary records of Clement and Kent (1986, 1991).

CALS7K.2 is a continuous global model for the last 7000 years determined by a regularized least squares fit to archaeomagnetic and palaeomagnetic data using spherical harmonics in space and cubic B-splines in time. We follow the approach of Brown et al. (2007) and take the field structure of CALS7K.2 and examine the effects on the surface field morphology by scaling the magnitude of the axial dipole component linearly with time.

5.1. Palaeodirectional and palaeointensity variations

All three sections from La Palma sample the reversed and normal field either side of the main polarity change. Unfortunately, only one flow from the AS section (AS14) records the transitional field during the main polarity change; however, another flow from (AS7) records an equatorial virtual geomagnetic pole (VGP) at a time before the main polarity change (Fig. 12). Without $^{40}Ar/^{39}Ar$ dates

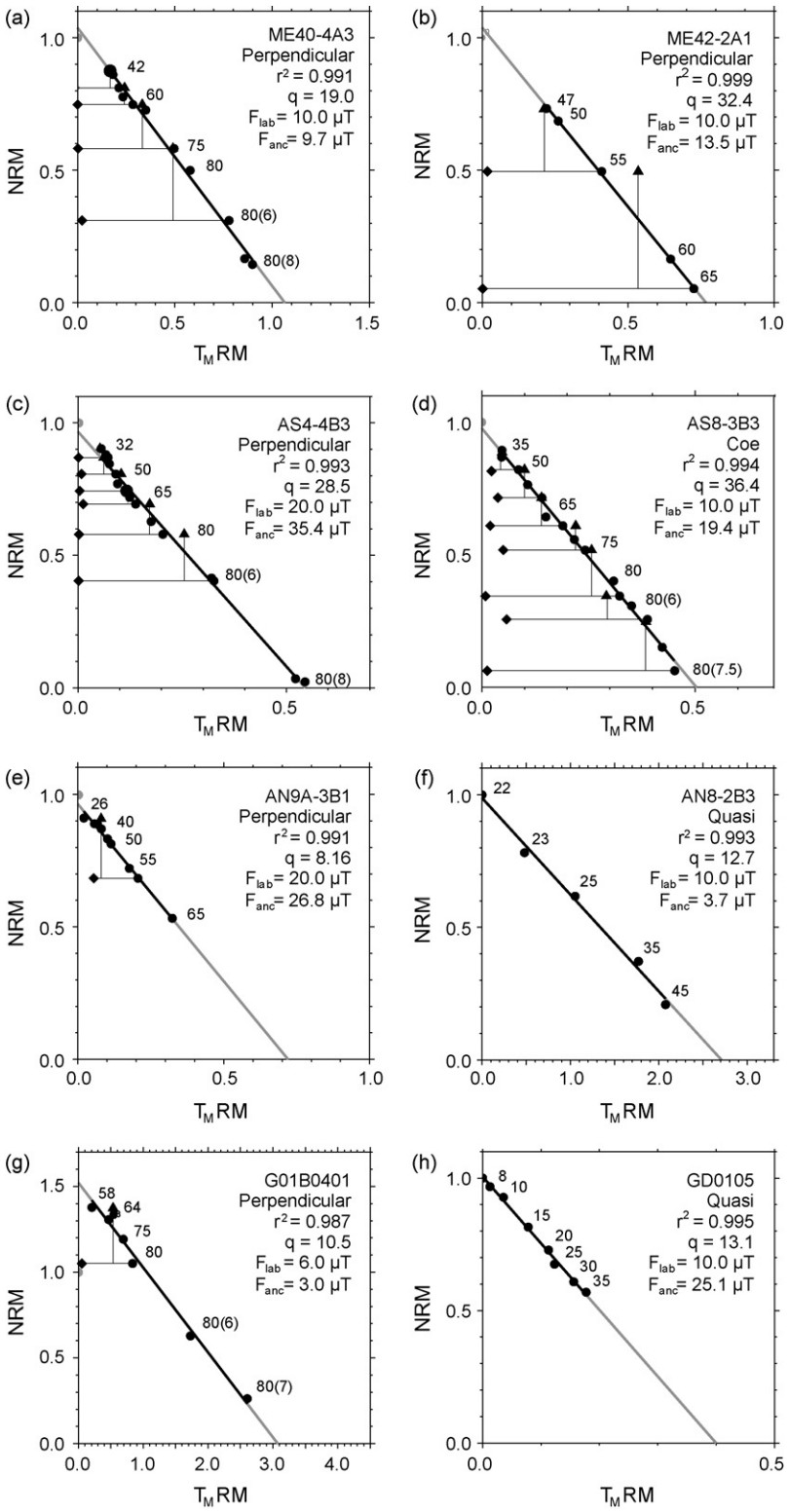

Fig. 10. Examples of Arai-Nagata plots (Nagata et al., 1963) for the La Palma (a–f) and Guadeloupe (g and h) sections. (a) and (c) Show 1st class results, (b, d–h) show 2nd class results. r^2 and q are defined in Section 3.4. F_{lab} is the applied field during the palaeointensity experiment and F_{anc} is the palaeointensity estimate. Numbers accompanying the data points are the microwave power steps in watts. The numbers in brackets are time in seconds; where no bracketed numbers are shown, the time of application was 5 s. Perpendicular denotes that the perpendicular applied method was used; Coe, the double-heating method (Coe, 1967); Quasi, the quasi-perpendicular applied field method (Biggin et al., 2007b). Examples (f) and (h) were determined using the quasi-perpendicular method, so no pT_MRM checks or tail checks were used. Quasi-perpendicular experiments were performed on the Tristan 14 GHz system, which has a more efficient cavity, so the amount of power needed to de(re)magnetise the sample was much less.

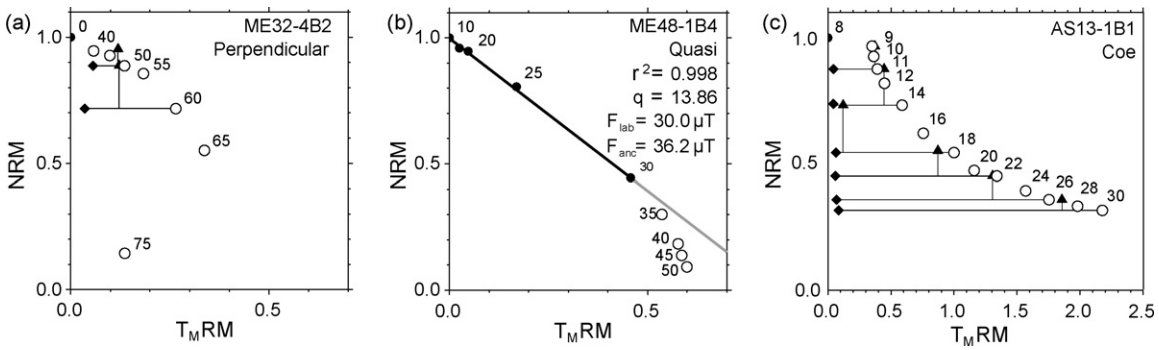

Fig. 11. Examples of Arai-Nagata plots which fail the palaeointensity experiments (a and c) or have unusual non-ideal characteristics. Graph labels are explained in Fig. 10.

for these two flows it is not possible to determine which stage of the reversal these transitional directions belong to. AS7 could record part of the precursor event relating to the MB reversal (Singer et al., 2002, 2005) or an earlier excursion at 821 ± 13 ka (Quidelleur et al., 2003). The date of the excursion also corresponds with the dated flows from the TS section prior to the main polarity change (Singer et al., 2002)(Fig. 12) and also with a transitional direction from western Mexico (dated at 819 ± 2 ka (Petronille et al., 2005). It is also not clear whether this excursion is also part of the MB reversal (Gratton et al., 2007). AS14 could record the precursor, as determined for flows 17 and 18 from the TN section of Singer et al. (2002), or the main polarity change. Although Quidelleur et al. (2002, 2003) and Singer et al. (2002) dated many flows from both the AS and AN sections, they did not record either of the transitional directions determined in this study (Fig. 12). All three studies show differences in the number of flows sampled and the directional results obtained. We attribute this discrepancy to difficulties in re-identifying flows from previous studies in the field and also to the large number of flows which were often hard to delimit.

VGP paths from the three La Palma sections are quite different (Fig. 13a–c); however, these differences result from the discrete nature of the flows in each sequence and do not represent the behaviour of the field between VGPs. Each volcanic

Table 1
Mean microwave palaeointensity results per flow for the ME, AS and AN sections from La Palma and the Guadeloupe section, West Indies. *All estimates* takes all classes, 2 and 3 results; *classes 1 and 2 estimates* takes all estimates that pass the classes 1 and 2 selection criteria (Section 3.4). *n* is the number of estimates used to calculate the flow mean. Mean *F* is the mean palaeointensity; σ_F is one standard deviation of the flow mean intensity; VDM is the flow mean virtual dipole moment; σ_V is the standard deviation of the flow mean VDM. R.S.D. (%) is the relative standard deviation of the flow.

Flow number	All estimates						Class 1 and 2 estimates					
	n	Mean *F* (μT)	σ_F (μT)	VDM × 10^{22} (A m²)	σ_V × 10^{22} (A m²)	R.S.D. (%)	*n*	Mean *F* (μT)	σ_F (μT)	VDM × 10^{22} (A m²)	σ_V × 10^{22} (A m²)	R.S.D. (%)
ME section, La Palma												
32	7	36.1	10.7	8.3	2.4	29.6	4	35.0	10.2	8.1	2.4	29.1
36	3	12.1	3.1	2.5	0.8	25.6	1	16.4		3.4		
39	4	11.3	3.1	2.9	0.8	27.4	0					
40	6	10.3	1.8	2.6	0.5	17.5	4	10.5	2.1	2.7	0.5	20.0
42	4	15.8	2.1	4.0	0.5	13.3	4	15.8	2.1	4.0	0.5	13.3
44	3	15.7	4.3	4.0	1.1	27.4	1	13.1		3.4		
47	10	36.6	12.2	8.8	2.9	33.3	5	42.1	10.0	10.1	2.4	23.8
48	14	41.4	10.5	9.5	2.4	25.4	8	37.7	5.9	8.7	1.4	15.6
49	8	30.3	13.8	6.9	3.2	45.5	3	44.2	8.1	10.1	1.9	18.3
AS section, La Palma												
4	1	35.4		7.9			1	35.4		7.9		
8	3	17.1	2.0	4.0	0.5	11.7	1	19.4		4.6		
12	3	3.0	1.3	0.7	0.3	43.3	1	4.3		1.1		
14	4	10.0	3.1	1.9	0.6	31.0	4	10.0	3.1	1.9	0.6	31.0
17	4	16.3	7.0	3.3	1.4	42.9	1	14.7		3.0		
18	5	14.6	8.5	3.3	1.9	58.2	1	4.3		1.0		
19	12	6.9	6.1	1.3	1.2	88.4	8	6.3	5.1	1.2	1.0	81.0
20	5	3.6	2.9	0.9	0.7	80.6	1	9.7		0.6		
AN section, La Palma												
1	3	2.4	0.8	0.5	0.2	33.3	0					
2	2	9.6		2.4			1	7.5		1.8		
3	5	6.9	3.3	1.7	0.8	47.8	3	7.1	4.2	1.8	1.0	59.2
6	1	4.8		0.7			1	4.8		0.7		
7	2	12.3		2.8			0					
8	4	5.3	2.5	1.0	0.5	47.2	1	3.7		0.7		
9	4	22.8	3.5	4.0	0.6	15.4	3	22.3	4.2	3.9	0.7	18.8
12	1	31.7		7.2			0					
Guadeloupe section, West Indies												
1	2	22.1		5.1			2	22.1		5.1		
2	5	5.1	1.6	1.3	0.4	31.4	1	3.0		0.8		
3	4	14.7	4.6	2.4	0.8	31.3	1	17.0		2.8		
4	8	16.8	4.9	4.0	1.2	29.2	3	20.4	5.5	4.9	1.3	26.7

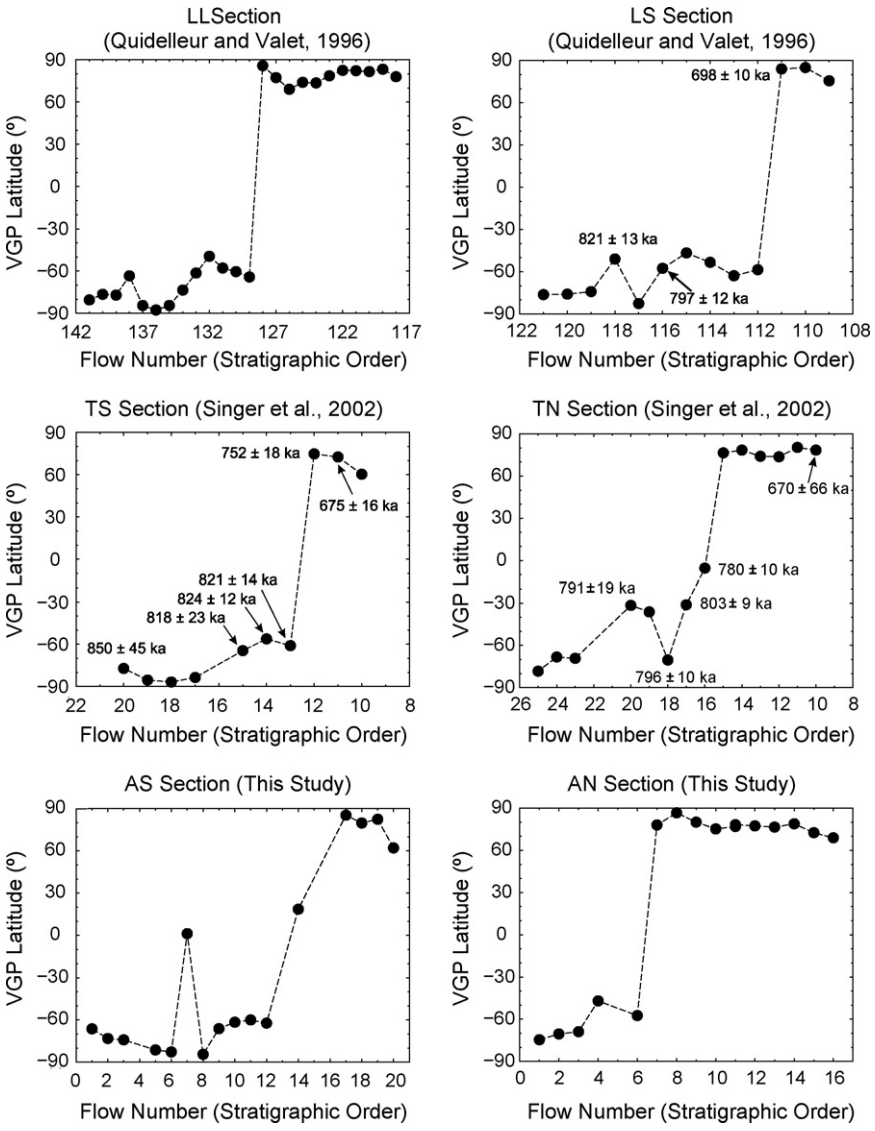

Fig. 12. Comparison of VGP latitude against flow number for the Barranco del Agua sections, La Palma. Errors on VGP latitude can be found in Quidelleur and Valet (1996) and Singer et al. (2002) and in Table A.2. Dates on the LS section are $^{40}K/^{40}Ar$; TS and TN dates are $^{40}Ar/^{39}Ar$.

sequence records part of a transitional field that is more complex than indicated by any of the three records. The problem of assessing VGP paths (and the complexity of all directional changes) from volcanic sequences is highlighted when compared with the results generated for La Palma by IMMAB4 (Leonhardt and Fabian, 2007)(Fig. 13f). Our new directional results do not match the results from IMMAB4 in detail (Fig. 13a–c and f); however, the incorporation of sedimentary records in this model has greatly increased the detail that can be resolved for the reversal recorded on La Palma. Without analysis of sedimentary records in accompaniment to volcanic records the recorded transitional field behaviour can be simplified and misinterpreted. Such possible complexity in directional changes for the MB reversal is seen in the sedimentary records of Channell and Lehman (1997) and Yamazaki and Oda (2001), which both show multiple polarity changes and other large directional variations before the final polarity change. This behaviour has also been seen for a number of other reversals recorded in sedimentary sequences (see Coe and Glen, 2004 and references therein). However, problems in the sedimentary recording mechanism and the fidelity of sedimentary records must always be considered. In addition, both volcanic and sedimentary records will always be incomplete and can only give a lower bound on the amount of directional and intensity variation for any particular reversal (Coe and Glen, 2004).

The palaeointensity results determined from the ME section using the microwave technique are in broad agreement with those determined by Valet et al. (1999) using the thermal Thellier method (Fig. 14). When no selection criteria are used the results from all flows agree (to within 2σ) with the exceptions of ME36, ME38 and ME39 (Fig. 14a). For two flows only one thermal Thellier or microwave determination was possible. For the third flow (ME39) the thermal Thellier result is 2.5 times greater. The individual microwave results from this flow were all class 3 and only one thermal Thellier result passed the class 1 selection criteria. Results from this flow are deemed unreliable. When the microwave flow mean palaeointensities are compared with the flow means determined using the thermal Thellier method for the three normal flows (ME47, ME48 and ME49), the means are comparable; however there is a larger range of individual palaeointensity results determined using the microwave technique. Only the comparisons to ME48 and ME47 are statistically significant, as only two determinations were made using the thermal Thellier method for

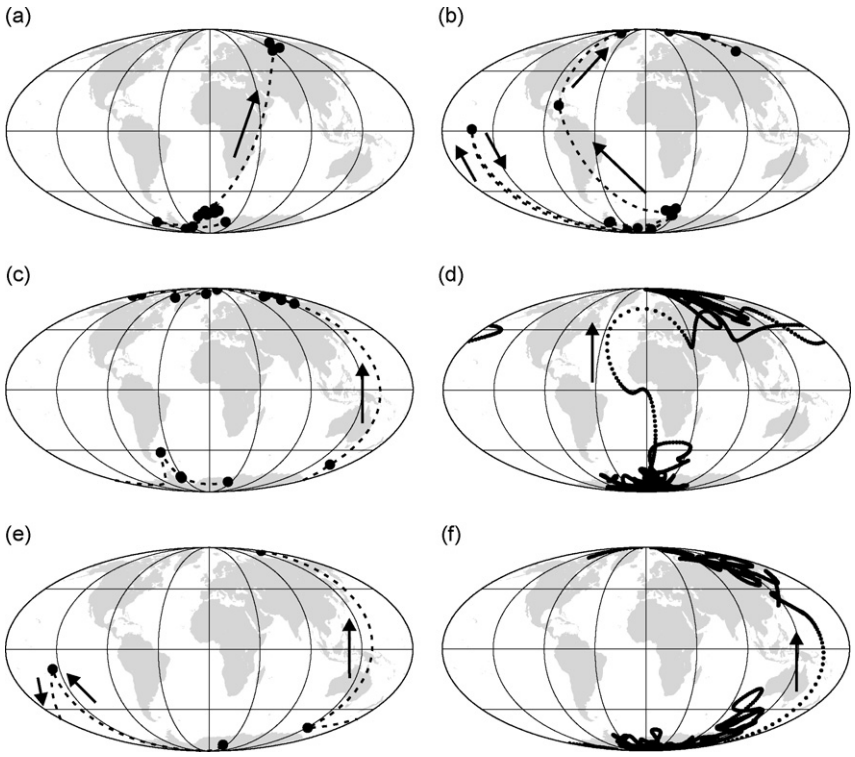

Fig. 13. Calculated VGP paths from palaeomagnetic data from (a) ME, (b) AS, (c) AN sections from La Palma and (e) Guadeloupe. Dashed lines indicate portions of great circles between VGPs. (d) VGP paths for La Palma and (f) Guadeloupe, generated by IMMAB4 (Leonhardt and Fabian, 2007), with each dot at 10-year intervals.

ME49. For ME48 the range of determinations using the microwave technique is 36.9 μT compared with 5.8 μT for the thermal Thellier technique; for ME47 the range of determinations using the microwave technique is 35.5 μT compared with 8.3 μT for the thermal Thellier technique. When the class 1 and 2 selection criteria are applied to both data sets the mean palaeointensities from the three normal polarity flows are no longer in good agreement (Fig. 14b).

Palaeointensity was only obtained for one transitional flow on La Palma (AS14) giving a value of 10 ± 3.1 μT ($n = 4$), corresponding to a virtual dipole moment (VDM) of $1.9 \pm 0.6 \times 10^{22}$ A m^2. Before the main polarity change the ME section gives a mean VDM of $3.4 \pm 0.53 \times 10^{22}$ A m^2 and the AS/AN sections give a mean VDM of $1.48 \pm 0.52 \times 10^{22}$ A m^2 (determined using all class 1 and class 2 data). This result is 2.3 times lower than the results from the ME section. It has already been noted in Section 2.1 that the palaeointensity results from the ME section (Valet et al., 1999) appear anomalously high when compared to the PINT03 database (Perrin and Schnepp, 2004) and this is again seen in our study. One possibility for this discrepancy is that the ME section and AS/AN sections were erupted at different times and capture different parts of the reversal; the AS/AN sections recording times when the field was at a minimum and the ME section recording times, possibly earlier in the reversal's history, when the palaeointensity was higher. Another possibility is that these palaeointensities are erroneous and this is related to the samples' oxidation state. Yamamoto et al. (2003) determined overestimated palaeointensities from samples from the 1960 Hawaii lava flow. They observed that these samples had undergone intermediate oxidation on initial cooling below their Curie temperature and that they could have acquired a thermochemical remanent magnetisation (TCRM). No microscopy was done in this study so such bold conclusions cannot be drawn; however, variations in the composition and the low-temperature properties of samples from the same flows and the same 25 mm cores suggest that some oxidation of these samples has occurred and that it was not homogeneous. Nevertheless, all La Palma sections show a decrease in palaeointensity during the directional changes (Fig. 15) and low palaeointensities have been recorded in flows that record both normal and reversed directions.

The directional record from Guadeloupe shows a reversed-transitional-reversed-normal progression with time (Fig. 13d). The transitional-reversed-normal progression was also recorded by Carlut et al. (2000); however, our directional results differ. For the transitional and reversed flows the two sets of results are comparable (within the 95% cone of confidence); however, for the normal flow there is a discrepancy. The mean direction for this flow from this study is $D = 353.8^\circ$, $I = 24.2^\circ$ ($N = 4$) compared with the equivalent result of flow GU11 (Carlut et al., 2000) of $D = 340.7^\circ$; $I = 31.4^\circ$ ($N = 9$).

The palaeointensity results from the two flows of Carlut and Quidelleur (2000) determined by the thermal Thellier method are significantly different to the microwave results determined in this study. Both the flows gave higher palaeointensities when determined using the microwave technique. For G02 (FN3) (G10; Carlut and Quidelleur, 2000) there is a difference of 12.8 μT and for G03 (FN4) (GU1) there is a difference of 11.1 μT. Only one sample from all the Carlut and Quidelleur (2000) flows passes the classes 1 and 2 selection criteria, and although the quality of the microwave results is generally low, it has improved upon the results from the original study.

^{40}K/ ^{40}Ar dating of the flows studied in Carlut et al. (2000) and Carlut and Quidelleur (2000) ranges from 777 ± 14 ka ($\pm\sigma$) to 785 ± 22 ($\pm\sigma$) ka. The VGP calculated from the transitional flow is very similar to that recorded by AS7 from La Palma. The errors on the dating, the agreement of VGPs and the reversed-transitional-reversed trend could suggest that the transitional flow records the precursor to the main polarity change at 793 ± 3 ka (Singer et al., 2005) or possibly an earlier excursion. Although the quality of the

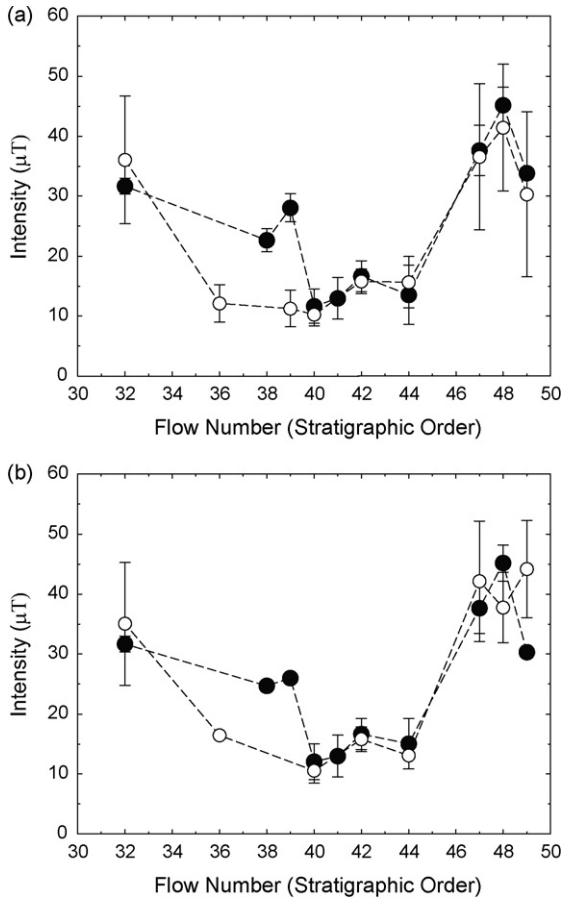

Fig. 14. Comparison of microwave flow mean palaeointensity results from this study (open circles) and thermal Thellier results from Valet et al. (1999) (closed circles). (a) All estimates of palaeointensity. (b) Palaeointensity results that pass the class 1 and class 2 selection criteria. Error bars are $\pm\sigma$.

palaeointensity data determined for the transitional-reversed part of the Guadeloupe sequence is poor, the VDM remains low (below 3×10^{22} A m^2) during this time (Fig. 15d). This result is consistent with VDM values determined from the precursor event recorded in the Tatara-San Pedro lavas, Chile (Brown et al., 2004; Gratton et al., 2007). The Tatara-San Pedro section consists of a series of lavas that record very similar directions, with VGPs that cluster over Australia. ^{40}Ar/ ^{39}Ar dates place this VGP cluster at 791.7 ± 3 ka. It has been suggested that during the reversal there is sustained field behaviour related to mantle-controlled magnetic flux patches (Hoffman and Singer, 2004), which leads to clustering of VGPs. Such clusters have also been determined for a number of other reversal records (Mankinen et al., 1985; Hoffman, 1992, 1996; Glen et al., 1994, 2003). Consistent directions could have been recorded by rapidly erupted lavas with no requirement for another physical mechanism; however, debate about the meaning of the geochemical analysis (Dungan et al., 2001), rock magnetic results (Brown et al., 2004; Gratton et al., 2007), and our understanding of long-lived geochemical systems means that both hypotheses remain for this section.

Error in dating the normal flow from Guadeloupe means that it is not clear if this flow records the post-reversal normal field or part of the precursor event. Although VDM is seen to increase (4.9 ± 1.3 ($\pm\sigma$) $\times 10^{22}$ A m^2) (Fig. 15a), this could be associated with the precursor, as seen in sedimentary records (Hartl and Tauxe, 1996) and possibly in the Tatara-San Pedro volcanic sequence (Gratton et al., 2007). The temporal evolution of the Guadeloupe and Tatara San Pedro sections is very difficult to interpret due to the

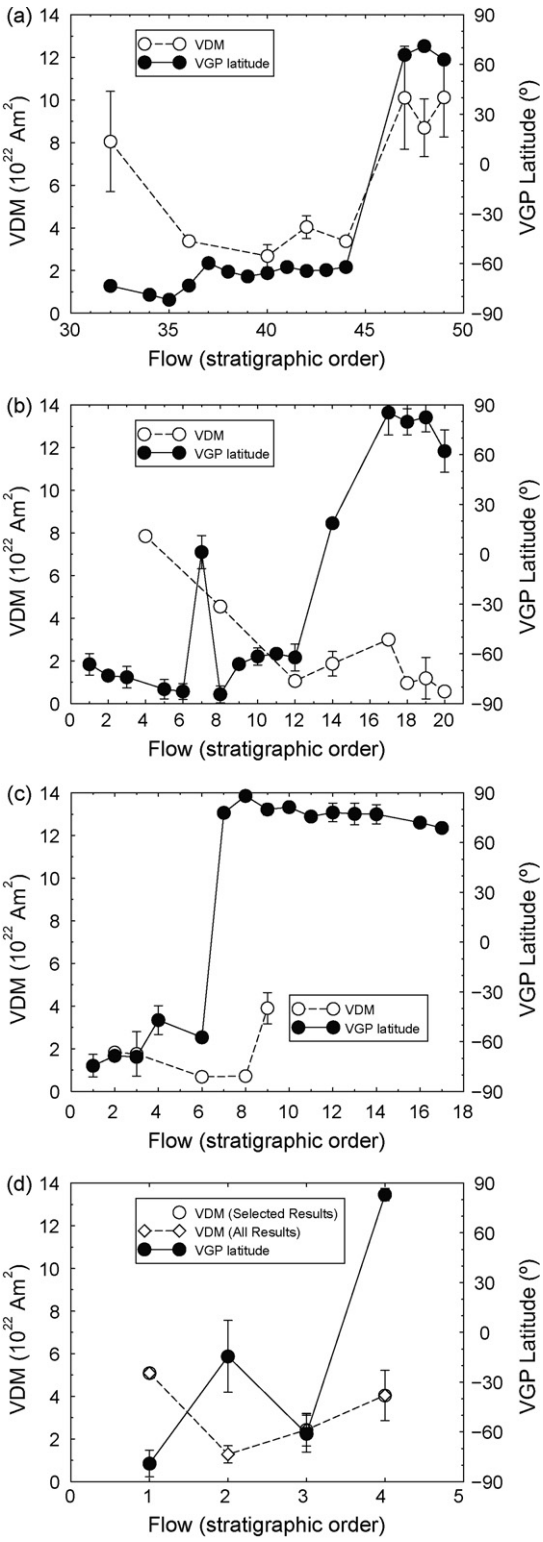

Fig. 15. VGP latitude and VDM plots for (a) ME, (b) AS, (c) AN and (d) Guadeloupe sections. VDM determinations for ME, AS, AN sections are from class 1 and 2 determinations; VDM determinations for the Guadeloupe section show both VDM determinations from all classified data (open diamonds) and classes 1 and 2 data (open circles). VDM error bars are σ_v and are shown in Table 1. VGP latitude errors are *dm* (Butler, 1992). Where no error bars are present the palaeomagnetic result was determined from less than three samples.

discrete nature of the sampling. The interpretation is further complicated by the possible speed of directional changes. Leonhardt and Fabian (2007) determined from IMMAB4 that local field directions can rotate very quickly (up to 2.2°/year), a feature that has been generated in dynamo simulations (Coe et al., 2000) and simple mathematical models of reversals (Brown et al., 2007). Rapid changes in the field have been suggested to explain the palaeomagnetic record of Steens Mountain (Mankinen et al., 1985); however, these changes were more rapid, with maximum changes between 3 and 10°/day (Coe and Prévot, 1989; Coe et al., 1995). This behaviour is thought to be significantly site dependent (Clement, 2004; Wicht, 2005; Brown et al., 2007; Leonhardt and Fabian, 2007).

IMMAB4 does not resolve the precursor in direction before the main polarity change (Fig. 13e and f); however, a broad decrease in intensity is seen between 790 ka and 780 ka before a peak in intensity prior to low field values during the main polarity change (Leonhardt and Fabian, 2007 do note the model is less reliable for dates > 782 ka). This intensity variation, but not a polarity change, is (unsurprisingly) seen in the sedimentary and volcanic records of Valet et al. (1989, 1999). The difference between the records could be caused by non-uniformity in the timing and the size of the global reduction in the field during this time; however, low intensity approximately 16 ka before the main polarity change has been observed globally (Schneider et al., 1992; Meynadier et al., 1994; Hartl and Tauxe, 1996; Dinarès-Turell et al., 1999).

The precursor event recorded in lavas at 793 ± 3 ka could relate to the initial onset of geodynamo instability (Singer et al., 2005), resulting in a reduction in the relative strength of the large-scale dipole contributions and an emergence of non-dipole contributions at the Earth's surface. Geodynamo instability could result from an emergence of magnetic upwellings (generated within buoyancy driven upwellings in the outer core, but with little or no dramatic change in fluid flow; Wicht and Olson, 2004), which amplify and transport a generally multipolar magnetic field from the inner boundary to the core-mantle boundary (Aubert et al., 2008).

5.2. Comparison with other Matuyama–Brunhes data

To compare palaeodirection and palaeointensity results from multiple global locations we characterise all results as VGPs and VDMs. We recognise the limitations of this approach. The assumption that the field is a geocentric dipole during the reversal (Merrill and McFadden, 1999) is certainly flawed due to the observation of various VGP paths for the MB reversal. Results from this study and all published MB data are shown in Fig. 16a and b. A clear feature is the rather simple relationship between variations in VGP and VDM. There are two broad groups: data that lie between $\pm 90°$ and $\pm 60°$ VGP latitude and data that lie between $-60°$ and $60°$ VGP latitude. Within the two high latitude bands VDM varies greatly, with VDMs at high VGP latitude both higher and lower than the present day dipole moment (7.9×10^{22} Am^2 calculated from the CHAOS geomagnetic field model; Olsen et al., 2006). Low values relate to times before and after the main polarity transition, where the dipole field is reduced in its strength but major directional changes have not occurred. This supports the idea that major directional changes have a shorter duration than intensity variations related to the reversal (Lin et al., 1994; Merrill and McFadden, 1999). All major directional changes ($-60°$ to $60°$ VGP latitude)

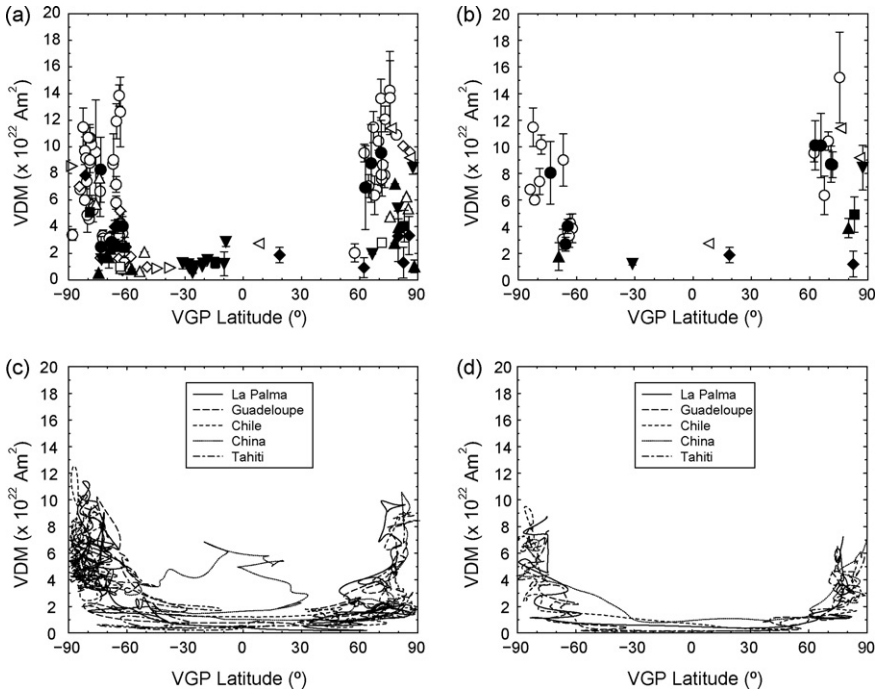

Fig. 16. (a) VDM versus VGP for all Matuyama–Brunhes data (number of determined means = 121). All estimates from this study and all other published data. No selection criteria were applied and many flow means were determined from less than three results. (b) VDM versus VGP for selected Matuyama–Brunhes data with three or more determinations per flow ($n = 31$). The class 1 and 2 selection criteria was imposed on data from this study. Previously published data were assessed on the published statistical parameters and where possible the class 1 selection criteria from this study were applied. This includes the removal of any data that used the Valet et al. (1996) palaeointensity correction. (a-b) Solid circles are microwave data and open circles are thermal Thellier data; solid circles: ME section (this study); open circles: ME and ET section (Valet et al., 1999); solid diamonds: AS section (this study); open diamonds: LL section (Quidelleur and Valet, 1996); solid upwards triangles: AN section (this study); open upwards triangles: LS section (Quidelleur and Valet, 1996); solid squares: Guadeloupe section (this study); open squares: Guadeloupe section (Carlut et al., 2000; Carlut and Quidelleur, 2000); solid downward triangles: Tartara San Pedro sections, Chile (Brown et al., 2004; Gratton et al., 2007); left pointing triangles: Tongjing basalts, China (Zhu et al., 1991); right pointing triangles: Punaruu Valley, Tahiti (Chauvin et al., 1990). (c) VDMs and VGPs generated by IMMAB4 (Leonhardt and Fabian, 2007) for locations shown in (a) and (b). (d) VDMs and VGPs generated by a simple reversal model based on CALS7K.2 (Korte and Constable, 2005; Brown et al., 2007) for the location shown in (a) and (b).

are coincident with VDMs less than 3×10^{22} A m^2 (approximately 35% of the present day globally averaged dipole moment). This suggests that the dipole moment needs to be reduced to at least this value before major directional instability occurs due to the emergence of dominant non-dipolar fields. Our interpretation of the MB is severely limited by the lack of data, especially if only flows with three or more palaeointensity determinations are included (Fig. 16b).

We compare the MB dataset with IMMAB4 transitional field structure dominated by the quadrupole with a reduced dipole contribution (Leonhardt and Fabian, 2007)(Fig. 16c). For all locations except China, the general banding of VGPs and VDMs is observed. The generation of high VDM at equatorial VGP latitudes is inconsistent with our data. Our analysis is clearly restricted by the characterisation of the data as VGPs and VDMs, which does not allow an assessment of the dominant non-dipolar terms. In addition, the data for a number of locations is considered from areas not included in the original model. In this case the model needs to be refined with additional data.

We have carried the same analysis using the simple reversing axial dipole model of Brown et al. (2007) based on CALS7K.2 (Korte and Constable, 2005). We again see the banding of VGPs and VDMs in the simulated reversal; however, generated VDMs are lower at transitional VGP latitudes. This is because CALS7K.2 underestimates the likely strength of the non-dipole field as the model has very little resolution above spherical harmonic degree four (C. Constable, personal communication).

6. Conclusions

The microwave technique has been used to determine a fragmentary record of the evolution of geomagnetic field intensity through the Matuyama–Brunhes geomagnetic field reversal recorded in three sections on La Palma, and one section on Guadeloupe. These sections record the main polarity transition, possible precursors, and fluctuations in the magnetic field prior to the main polarity reversal; however, it has proved difficult to obtain robust palaeointensity determinations. Only 10 flows from the 29 flows studied gave reliable mean palaeointensities with three or more determinations per flow. Of these 10 flows, only 1 records a transitional direction. The VDM determined from this flow is 1.9 ± 0.6 ($\pm\sigma$) $\times 10^{22}$ A m^2. Analysing both thermal Thellier and microwave palaeointensity results from all Matuyama–Brunhes studies suggests that the main directional changes occurred once the VDM was reduced below 3×10^{22} A m^2. However, the lack of transitional data does not allow us to make any robust statements about the transitional field behaviour. To understand the reversal process and how this links to geodynamo behaviour, more accurate transitional palaeointensity determinations are required. In addition detailed radiometric dating is needed to clearly determine the temporal variation and complexity of reversal features recorded in volcanic sections and, where more than one record exists for a particular reversal, correlate them globally.

Acknowledgements

This work was carried out under NERC grants NER/S/J/2004/13080 and NERC/A/S/2003/00330 and a visiting fellowship to the Institute for Rock Magnetism, University of Minnesota. The microwave instrumentation was funded by NERC grant NE/B50572X/1. The Institute for Rock Magnetism is supported by a grant from the Instruments and Facilities program, Earth Science Division, the National Science Foundation. Roman Leonhardt and Karl Fabian are thanked for their time and for providing us with the code for the IMMAB4 model. Monika Korte is thanked for providing the CALS7K.2 model. Elisabeth Schnepp and an anonymous reviewer are thanked for their comments. Edward Horncastle, Amy Chen, Yuhji Yamamoto, Mimi Hill, Neil Suttie, Mike Jackson and John Share are thanked for scientific discussions and their experimental assistance. We would like to thank the Medio Ambiente of Santa Cruz de La Palma for providing us with sampling permits.

Appendix A. Palaeodirection results

See Tables A.1–A.4 .

Appendix B. Palaeointensity results

See Tables B.1–B.4 .

Table A.1
Palaeodirection results for the MB reversal from the ME section, La Palma. Flow Number labels individual lava flows and is the number shown in any figure relating to palaeodirection or palaeointensity results. *I* is inclination; *D* is declination; M.A.D. is maximum angular deviation (Kirschvink, 1980); Temp range is the temperature interval taken for the directional analysis of the primary component of magnetisation; Accept is whether the individual sample was included in the flow analysis; Flow *I* is the mean inclination; Flow *D* is the mean declination; α_{95} is the angular standard deviation (Fisher, 1953; Butler, 1992); κ is the precision parameter (Butler, 1992); VGP Lat. is the virtual geomagnetic pole latitude and VGP Long. is the virtual geomagnetic pole longitude (Butler, 1992).

Sample	Flow number	*I* (°)	*D* (°)	M.A.D. (°)	Temp range (°C)	VGP Lat. (°)	VGP Long. (°)
ME30-3B	30						
ME31-4B	31						
ME32-4B	32	−31.6	167.0	3.8	350–525	−73.4	30.8
ME34-3A	34	−33.6	184.9	1.9	350–525	−78.8	317.5
ME35-5B	35	−41.4	187.3	5.1	450–525	−81.8	287.1
ME36-2A	36	−43.9	198.6	3.1	450–525	−73.2	257.9
ME37-1A	37	−1.3	168.0	3.4	350–525	−59.7	6.4
ME38-5A	38	−7.4	177.3	4.0	300–525	−64.9	348.4
ME39-5A	39	−12.7	180.5	6.1	400–525	−67.8	340.7
ME40-2A	40	−9.9	174.2	2.1	400–525	−65.7	356.2
ME41-1B	41	−7.9	166.3	3.8	400–525	−62.1	12.4
ME42-2B	42	−8.1	173.0	3.5	350–525	−64.5	358.5
ME43-4B	43	−9.3	169.2	5.7	450–525	−63.9	7.2
ME44-5B	44	−2.5	174.7	4.8	350–525	−62.1	353.4
ME45-1B	45						
ME46-1A	46						
ME47-4B	47	25.1	20.0	2.5	350–525	65.8	107.7
ME48-2A	48	31.2	16.1	2.7	350–525	71.1	107.2
ME49-2A	49	32.0	26.8	2.9	400–525	62.9	90.9

Table A.2
Palaeodirection results from the AS section, La Palma. Where no result is shown, it was not possible to determine a primary component of magnetisation. Flow *I* is the mean inclination; Flow *D* is the mean declination; α_{95} is the angular standard deviation (Fisher, 1953; Butler, 1992); κ is the precision parameter (Butler, 1992); VGP Lat. is the virtual geomagnetic pole latitude and VGP Long. is the virtual geomagnetic pole longitude (Butler, 1992); *dm* is the confidence limit for VGP latitude and *dp* is the confidence limit for VGP longitude (Butler, 1992). See Table A.1 for explanation of other column headings.

Sample	Flow number	*I* (°)	*D* (°)	M.A.D. (°)	Temp range (°C)	Accept	Flow *I* (°)	Flow *D* (°)	α_{95} (°)	κ	VGP Lat. (°)	VGP Long. (°)	*dm* (°)	*dp* (°)
AS1-1	1	−19.8	157.8	4.2	200–525	Y								
AS1-2		−21.7	156.2	9.8	150–525	Y								
AS1-3		−33.6	157.8	4.4	450–525	Y								
AS1-4		−34.5	163.3	3.6	200–525	Y								
AS1-5		−29.4	161.9	8.4	150–525	Y	−27.8	159.3	6.9	124.8	−66.3	40.4	6.5	7.5
AS2-1	2	−32	193.5	4.1	400–525	Y	-32	193.5			−73.1	292.1		
AS3-1	3	−4.7	205.3	5.4	250–525	N								
AS3-3		−33.3	161.6	4.5	0–525	N								
AS3-4		−28.9	198.3	2.0	150–525	Y								
AS3-5		−29.4	167.8	1.6	250–525	N								
AS3-6		−31.7	196.5	7.0	150–525	Y	−30.3	197.4			−74.1	286.5	6.4	7.8
AS4-1	4	−14	224.6	1.7	100–525	N								
AS4-2		−44.6	170.8	7.4	350–525	N								
AS4-3		−45.9	114	1.3	400–525	N								
AS5-1	5	−39.9	173.4	3.9	250–525	Y								
AS5-2		−33.2	188.3	3.7	150–525	Y								
AS5-3		−35.8	178.9	2.9	400–525	Y								
AS5-4		−35.5	182.6	3.0	350–525	Y	−36.2	181	6.5	197.9	−81.3	336.3	5.8	7.6
AS6-1	6													
AS6-3		−38.9	179	5.5	350–525	Y								
AS6-4		−37.1	173.6	0.3	400–525	Y								
AS6-5		−39.5	170.1	17.3	350–525	Y								
AS6-6		−44.9	178.7	1.2	400–525	Y	−40.2	175.3	5.3	298.8	−82.7	19	4.8	6.4
AS7-1	7	−49.5	304.5	2.7	250–525	Y								
AS7-3		−59.6	292.7	5.4	400–525	Y								
AS7-4		−53.5	296.8	7.0	150–525	Y								
AS7-5		−67.2	294.3	3.1	250–525	Y	−57.3	297.7	9.4	96.7	1.3	206.4	10.0	13.7
AS8-1	8	−44.6	188.4	4.1	400–525	Y								
AS8-2		−48.7	188.4	2.9	250–525	Y								
AS8-3		−46.5	188.3	4.2	100–525	Y								
AS8-4		−35.8	178.9	2.9	400–525	Y								
AS8-5		−41.9	182.3	8.5	150–525	Y	−43.6	185	5.6	185.3	−84.4	288.1	5.1	7.0
AS9-1	9	−28.7	159.8	8.2	350–525	Y								
AS9-2		−29.5	158.3	9.5	250–525	Y								
AS9-3		−28	159.3	2.9	250–525	Y	−28.7	158.8	1.3	8692.2	−66.2	42.2	1.2	1.4
AS9-4														
AS9-5														
AS10-1	10													
AS10-2		−13.1	161	2.5	450–525	Y								
AS10-3		−17.3	157.3	4.3	300–525	Y								
AS10-4		−15.5	161	4.0	400–525	Y	−15.3	159.8	4.5	758	−61.6	28.4	5.2	4.6
AS11-1	11													
AS11-2		−21.2	153.9	4.3	400–525	Y	−21.2	153.9			−59.9	41.3		
AS11-4														
AS12-1	12	−22.7	166.2	5.1	350–500	Y								
AS12-3		−18.3	150.4	7.8	400–525	Y								
AS12-4		−16.2	157.3	6.7	400–525	Y								
AS12-5		−19.2	159.2	8.1	450–525	Y	−19.2	158.2	7.6	147.2	−62.2	33.8	8.0	7.9
AS13-1	13													
AS13-2														
AS13-3														
AS13-4														
AS14-1	14	52.7	274.5	2.5	300–550	Y	52.7	274.5			18.7	280.6		
AS15-1	15													
AS16-1	16													
AS16-2														
AS16-3														
AS16-4														
AS16-5														
AS17-1	17	42	17	7.4	350–500	Y								
AS17-2		46.3	351.1	1.0	100–550	Y								
AS17-3		43	3.4	5.3	350–550	Y	44.5	4.2	14.8	70.7	85.4	107.1	13.5	18.6

Table A.2 (*Continued*)

Sample	Flow number	I (°)	D (°)	M.A.D. (°)	Temp range (°C)	Accept	Flow I (°)	Flow D (°)	α_{95} (°)	κ	VGP Lat. (°)	VGP Long. (°)	dm (°)	dp (°)
AS18-1	18	32.7	358.7	6.6	350–550	Y								
AS18-2		32.6	41.7	5.9	350–550	N								
AS18-3		35.6	2.1	2.1	350–550	Y	34.2	0.4			79.9	160.2	7.9	10.1
AS19-1	19	48.7	344.1	1.3	400–550	Y								
AS19-2		52.3	351.8	2.3	400–550	Y								
AS19-3		43.6	18.3	5.3	350–500	N								
AS19-4		35	350	15.7	350–550	N								
AS19-5		52.6	52.6	2.4	350–550	Y	51.4	352.5	8.9	193.4	82.5	280	8.7	12.1
AS20-1	20	12.3	6.9	3.0	350–550	Y								
AS20-2		8.2	20.2	4.3	350–550	Y								
AS20-3		13.2	10.4	11.1	400–550	Y								
AS20-4		5	22.6	11.2	400–550	Y	9.7	15.1	9.5	93.9	62.2	128.5	12.7	9.6

Table A.3
Palaeodirection results for the MB reversal from the AN section, La Palma. Where no result is shown it was not possible to determine a primary component of magnetisation. See Table A.2 for explanation of column headings.

Sample	Flow number	I (°)	D (°)	M.A.D. (°)	Temp range (°C)	Accept	Flow I (°)	Flow D (°)	α_{95} (°)	κ	VGP Lat. (°)	VGP Long. (°)	dm (°)	dp (°)
AN1-1	1													
AN1-2		−30.3	162.4	3.6	100–525	Y								
AN1-3		−31	169.1	2.6	100–525	Y								
AN1-4		−37.9	172.5	3.2	100–525	Y								
AN1-5		−41	162.0	2.4	250–525	Y	−35.1	167	7.6	146	−74.5	37.8	6.8	8.8
AN2-1	2	−23.3	191.9	0.7	450–525	Y								
AN2-2		−17.4	192.2	2.9	400–525	Y	−20.3	192			−68.5	308.2		
AN3-1	3	−20.8	186.0	2.8	350–525	Y								
AN3-3		−14.2	187.4	2.4	350–525	Y	−17.5	187			−69.2	322.3		
AN4-1	4													
AN4-2														
AN4-3		18.4	202.3	3.7	450–550	Y								
AN4-4		14.3	207.1	3.5	450–550	Y								
AN4-5		10	203.5	2	450–550	Y	14.2	204	7.4	280	-47	305.4	8.7	7.6
AN6-1	6													
AN6-2														
AN6-3														
AN6-4														
AN6-5		−74.6	174.1	3.6	350–500	Y	−74.6	174			−57.4	156.9		
AN7-1	7	31.2	9.0	2.4	400–525	Y								
AN7-2		33.2	3.4	3.1	400–525	Y								
AN7-3		34.3	4.8	2.5	400–525	Y								
AN7-4		34.3	7.5	3.2	0–525	Y	33.3	6	2.9	984	77.9	132.8	2.6	3.3
AN8-1	8	46	2.3	2.7	0–525	Y								
AN8-2		50.5	1.8	3.4	0–525	Y								
AN8-3		−17.7	187.4	4.9	0–525	N	49.7	3			86.6	42.1		
AN9a-1	9	57.4	2.6	5	150–525	Y								
AN9a-2		59.9	3.2	2.9	350–525	Y								
AN9a-3		58.3	356.1	5	150–525	Y								
AN9a-4		56.1	5.8	0.6	450–525	Y	58	2	3.1	891	80	351.2	3.3	4.6
AN9b-1	10	54.9	2.2	3.1	100–525	Y								
AN9b-2		59.2	359.6	4.1	100–525	Y								
AN9b-3		56.2	355.9	6	100–525	Y								
AN9b-4		51.8	314.5	4.4	400–525	N	56.8	359	4.3	825	81.4	338.3	4.5	6.2
AN10-1	11													
AN10-2		30.9	5.6	3.9	100–550	Y								
AN10-3		27.3	6.1	6.8	200–550	Y	29.1	6			75.7	138.8	7.3	8.7
AN11-1	12	31.6	1.7	3	0–525	Y								
AN11-2		29.6	2.3	3.4	100–525	Y								
AN11-3		31.1	6.1	3	100–525	Y								
AN11-4		39.2	10.6	1.6	200–400	Y	32.9	5	6.2	219	78.2	138.1	5.6	7.0
AN12-1	13	29.3	354.7	2.1	350–550	Y								
AN12-2		27.5	355.6	1.3	450–550	Y								
AN12-3		36.4	356.3	2.4	450–550	Y	31.1	356	7.2	291	77.3	182.1	6.6	8.1
AN12-4														
AN13-1	14	27.2	6.4	5	350–550	Y								
AN13-2		29.7	9.4	4.1	150–550	Y								
AN13-3		39.7	5.8	3.5	250–550	Y								

Table A.3 (*Continued*)

Sample	Flow number	I (°)	D (°)	M.A.D. (°)	Temp range (°C)	Accept	Flow I (°)	Flow D (°)	α_{95} (°)	κ	VGP Lat. (°)	VGP Long. (°)	dm (°)	dp (°)
AN13-4		34.1	6.7	3.2	350–550	Y	32.7	7	6.4	206	77.1	130.1		
AN14-1	15	23.5	4.2	2.2	350–550	Y								
AN14-2		43.8	342.7	3.7	300–550	Y	34.1	355			78.8	188.8		
AN15-1	16	27.4	9.3	1.3	350–550	Y								
AN15-2		18.9	5.3	1.5	300–550	Y	23.2	7			72	138.0		
AN16-2	17													
AN16-3		17	7.3	0.3	500–550	Y	17	7			68.8	142.2		

Table A.4
Palaeodirection results for the MB reversal from Guadeloupe, French West Indies. See Table A.2 for explanation of column headings.

Sample	Flow number	I (°)	D (°)	M.A.D. (°)	Temp range (°C)	Accept	Flow I (°)	Flow D (°)	α_{95} (°)	κ	VGP Lat. (°)	VGP Long. (°)	dm (°)	dp (°)
GD0100	1	−27.6	144.2	2.7	0–350	Y								
GD0101		−26.9	161.3	4.3	100–350	Y								
GD0102		−33.4	181.3	5.2	100–350	Y								
GD0103		−31.8	168.8	5.1	100–350	Y								
GD0104		−29.1	170.4	5.7	150–350	Y								
GD0105		−28.4	177.4	4.1	150–350	Y								
GD0106		−38.5	178.2	2.9	0–350	Y	−31.4	168.6	8.8	47.8	-79	35.1	8.0	9.9
G01A01	2	10.1	233.5	3.5	300–540	Y								
G01A04		19.7	266.5	5.2	250–520	Y								
G01A06		12.9	90.8	2.6	300–520	N								
G01B02		−15.8	222.5	6.5	200–520	N								
G01C02		9.2	257.7	3.8	300–450	Y								
G01C07		6.3	255.4	4.8	200–520	Y	11.6	253.2	17.1	29.9	−14.4	218.8	21.6	17.4
G02A01	3	−47.7	174.8	16.7	400–540	N								
G02A03		−67.4	188	4.9	300–520	Y								
G02A04		−53.5	193.2	8.3	250–520	Y								
G02A06		−76.9	249.2	8.2	250–520	Y								
G02A07		−55.4	186.4	3.6	250–520	Y								
G02A08		−50.8	175.8	2.7	200–520	Y								
G02B04		−66.2	200.4	7.1	250–520	Y								
G02B05		−56.4	193.4	4.8	250–520	Y	−61.9	192.3	9.5	40.9	−61	136.9	11.1	14.7
G03A01	4	−8.9	0.2	2.4	200–520	N								
G03A03		22.3	351.3	4	100–540	Y								
G03A05		23.2	356.6	3.1	200–520	Y								
G03A07		24	351.4	2.2	200–520	Y								
G03A08		27.1	356.1	2.5	200–520	Y	24.2	353.8	3.8	579.5	83.1	179.1	3.7	4.1

Table B.1
Individual microwave palaeointensity results from the ME section, La Palma. Flow Number labels individual lava flows and is the number shown in any figure relating to palaeodirection or palaeointensity results. Flows are in stratigraphic order in ascending number from oldest to youngest (32–49). Demag indicates whether it was possible to resolve a primary component of magnetisation large enough to perform a palaeointensity experiment. Protocol is the experimental design chosen (protocols are explained in Section 3.3): Perp is the perpendicular applied field method (Kono and Ueno, 1977; Hill and Shaw, 2007); Coe is the double heating-method of Coe (1967); Quasi is the quasi-perpendicular applied method (Biggin et al., 2007b). F_{lab} is the laboratory applied field. n/N is the number of accepted NRM-pT_MRM points against the total number of pNRM-pT_MRM points determined from the palaeointensity experiment. f, g, β and q are Coe et al. (1978) quality statistics (see Section 3.4 for explanation of individual statistics and for further discussion). r^2 is square of the correlation coefficient (discussed in Section 3.4). pT_MRM check and Tail Check (explained in Section 3.4) columns show the number of checks that passed the selection criterion against the total number of checks relating to pNRM-pT_MRM points accepted for palaeointensity determination. F is the palaeointensity determination; uncert is the uncertainty of the individual palaeointensity determination using $(1/q)F$ (Coe et al., 1978); Class is explained in Section 3.4.

Sample	Flow number	Demag	Protocol	F_{lab}	n/N	f	g	β	q	r^2	pT_MRM check	Tail check	F (μT)	Uncert (μT)	Class
ME32-1B1	32	Y	Perp	40	7/7	0.47	0.64	0.06	5.18	0.983	1/1	1/1	37.5	7.2	2
ME32-2B1		Y	Perp	20	7/9	0.54	0.74	0.08	5.16	0.971	2/3	2/3	43.9	8.5	3
ME32-4B1		Y	Perp	10	6/6	0.60	0.49	0.03	10.22	0.997	2/2	0/2	47.7	4.7	2
ME32-4B2		Y	Perp	20	0/7										
ME32-4B3		Y	Perp	20	0/8										
ME32-4B4		Y	Perp	40	5/5	0.25	0.52	0.04	3.01	0.994	1/1	1/1	46.3	15.4	3
ME32-5B1		Y	Perp	40	6/6	0.58	0.33	0.01	19.72	1.000	2/2	2/2	23.3	1.2	1
ME32-5B2		Y	Perp	40	7/9	0.73	0.62	0.03	14.00	0.995	1/3	2/3	31.7	2.3	2
ME32-5B3		Y	Perp	40	4/4	0.35	0.29	0.04	2.46	0.997	0/0	0/0	22.0	8.9	3
ME33-2A1	33	Y	Perp	10	0/5										
ME33-5B1		Y	Perp	20	0/5										
ME34-4B1	34	N													
ME35-5B1	35	N													
ME36-1B1	36	Y	Perp	10	4/7	0.44	0.59	0.03	8.43	0.998	0/1	0/1	16.4	1.9	2
ME36-2B1		N	Coe												

Table B.1 (*Continued*)

Sample	Flow number	Demag	Protocol	F_{lab}	n/N	f	g	β	q	r^2	pT_MRM check	Tail check	F (μT)	Uncert (μT)	Class
ME36-3B1		Y	Perp	10	8/11	0.28	0.81	0.07	3.25	0.970	2/3	3/3	9.5	2.7	3
ME36-4B1		Y	Perp	40	8/11	0.13	0.78	0.07	1.32	0.967	4/4	4/4	10.4	7.9	3
ME36-5B1		N	Coe												
ME37-1B1	37	N													
ME38-1B1	38	Y	Perp	40	0/10										
ME39-4A1	39	Y	Perp	15	3/5	0.04	0.40	0.11	0.17	0.989	0/1	1/1	10.6	63.2	3
ME39-6C1		Y	Perp	40	6/7	0.73	0.45	0.03	11.76	0.997	2/2	2/2	15.8	1.3	3
ME39-6C2		N	Coe												
ME39-6C3		Y	Perp	40	5/5	0.43	0.01	0.07	0.08	0.987	1/1	1/1	9.7	123.0	3
ME39-6C4		Y	Perp	10	4/4	0.15	0.57	0.03	2.78	0.998	0/0	0/0	9.0	3.2	3
ME40-1A1	40	Y	Perp	10	9/9	0.59	0.72	0.03	14.09	0.993	2/3	3/3	13.0	0.9	2
ME40-2B1		Y	Perp	10	12/12	0.59	0.80	0.06	7.94	0.964	4/5	5/5	8.5	1.1	3
ME40-3A1		Y	Perp	10	11/11	0.68	0.86	0.02	31.27	0.997	5/5	4/5	8.2	0.3	2
ME40-3A2		Y	Perp	10	8/11	0.29	0.77	0.07	3.12	0.969	3/4	3/4	10.9	3.5	3
ME40-4A1		Y	Perp	40	0/11										
ME40-4A2		N	Coe												
ME40-4A3		Y	Perp	10	11/11	0.70	0.82	0.03	18.98	0.991	4/4	4/4	9.7	0.5	1
ME40-5A1		N	Coe												
ME40-5B1		Y	Perp	15	9/10	0.50	0.68	0.03	13.43	0.996	3/4	3/4	11.3	0.8	2
ME41-4A1	41	Y	Perp	10	0/4										
ME42-2A1	42	Y	Perp	10	5/5	0.66	0.65	0.01	32.43	0.999	1/2	2/2	13.5	0.4	2
ME42-3A1		Y	Perp	10	7/7	0.84	0.77	0.04	17.02	0.993	0/2	2/2	14.6	0.9	2
ME42-3A2		Y	Perp	10	5/5	0.76	0.74	0.02	24.15	0.998	0/2	2/2	17.1	0.7	2
ME42-5B1		Y	Perp	40	0/11										
ME42-5B2		N	Coe												
ME42-5B3		Y	Perp	40	7/7	0.50	0.77	0.04	10.77	0.994	3/4	4/4	17.9	1.7	2
ME43-5B1	43	N													
ME44-2B1	44	Y	Perp	40	5/5	0.38	0.71	0.14	1.94	0.944	0/2	2/2	20.6	10.6	3
ME44-2B2		Y	Perp	40	4/4	0.48	0.53	0.00	59.56	1.000	0/1	1/1	13.1	0.2	2
ME44-2B3		Y	Perp	40	5/7	0.15	0.59	0.08	1.09	0.980	0/3	3/3	13.3	12.2	3
ME45-1B1	45	N													
ME46-4B1	46	N													
ME47-1A1	47	Y	Perp	40	0/4										
ME47-1A2		Y	Quasi	30	0/3										
ME47-2A1		Y	Perp	40	8/8	0.59	0.59	0.01	55.05	1.000	2/2	2/2	40.3	0.7	1
ME47-2A2		Y	Perp	40	3/3	0.22	0.03	0.01	0.10	0.997	0/0	0/1	32.9	313.2	3
ME47-2A3		Y	Coe	40	5/6	0.77	0.50	0.02	15.76	0.998	1/2	1/2	50.7	3.2	2
ME47-2A4		Y	Coe	20	6/7	0.62	0.66	0.06	7.04	0.986	2/2	0/2	37.5	5.3	2
ME47-2B1		Y	Perp	40	5/5	0.70	0.58	0.05	8.11	0.994	2/2	2/2	28.8	3.5	1
ME47-3A1		Y	Perp	40	9/9	0.43	0.74	0.04	8.01	0.989	0/3	0/3	17.9	2.2	3
ME47-4A1		Y	Perp	40	5/8	0.31	0.62	0.05	4.81	0.995	1/1	1/1	50.2	10.4	3
ME47-4A2		Y	Perp	40	11/11	0.75	0.80	0.02	36.72	0.998	4/4	4/4	53.4	1.6	1
ME47-4A3		Y	Perp	30	7/7	0.28	0.69	0.01	13.23	0.988	1/2	1/2	31.6	2.4	3
ME47-4A4		Y	Coe	20	5/5	0.21	0.64	0.01	1.91	0.985	0/2	0/2	22.4	11.7	3
ME48-1B1	48	Y	Perp	40	11/11	0.79	0.78	0.01	72.07	0.994	4/4	1/4	34.6	0.5	2
ME48-1B2		Y	Perp	40	6/6	0.41	0.56	0.02	13.83	0.999	2/2	2/2	31.2	2.3	1
ME48-1B3		Y	Quasi	30	6/11	0.56	0.50	0.02	13.86	0.998	N/A	N/A	36.2	2.6	2
ME48-1B4		Y	Quasi	30	6/9	0.82	0.68	0.02	31.99	0.999	N/A	N/A	41.5	1.3	2
ME48-2A1		Y	Perp	40	13/14	0.84	0.77	0.01	41.20	0.999	4/5	1/5	35.4	0.9	2
ME48-2A2		Y	Perp	40	7/7	0.21	0.76	0.06	2.86	0.985	1/1	1/1	46.9	16.9	3
ME48-2A3		Y	Coe	40	7/7	0.39	0.59	0.03	7.00	0.995	3/3	1/3	24.8	3.5	3
ME48-2A4		Y	Perp	40	6/6	0.71	0.71	0.03	19.23	0.997	1/2	0/2	43.9	2.3	2
ME48-2A5		Y	Perp	40	7/17	0.04	0.81	0.07	0.51	0.978	3/3	1/3	46.1	89.6	3
ME48-3A1		Y	Perp	40	13/13	0.20	0.86	0.41	4.22	0.981	0/1	0/1	38.5	9.1	3
ME48-3A2		Y	Perp	40	9/9	0.76	0.69	0.02	22.57	0.996	1/1	1/1	47.4	2.1	2
ME48-3A3		Y	Perp	30	11/11	0.69	0.58	0.04	10.75	0.988	5/6	0/5	31.7	2.9	2
ME48-4A1		Y	Perp	40	5/6	0.72	0.39	0.03	8.00	0.996	0/1	0/1	61.7	7.7	3
ME48-4A2		Y	Perp	40	11/11	0.10	0.81	0.04	2.29	0.988	2/2	0/2	60.0	26.2	3
ME49-1A1	49	Y	Perp	40	7/7	0.44	0.71	0.06	4.94	0.980	1/3	2/3	17.9	3.6	3
ME49-2B1		Y	Perp	40	14/14	0.48	0.78	0.02	16.58	0.994	5/6	2/6	37.1	2.2	2
ME49-2B2		Y	Coe	40	5/6	0.14	0.57	0.11	0.75	0.964	1/2	1/2	16.1	21.4	3
ME49-2B3		Y	Quasi	30	6/6	0.91	0.79	0.06	12.62	0.987	N/A	N/A	53.0	4.2	2
ME49-2B4		Y	Quasi	30	7/8	0.95	0.82	0.03	27.69	0.996	N/A	N/A	42.4	1.5	2
ME49-3A1		Y	Perp	40	7/7	0.81	0.33	0.05	5.75	0.992	2/2	0/2	33.6	5.8	3
ME49-3A2		Y	Perp	15	7/7	0.60	0.47	0.04	7.06	0.994	2/2	1/2	27.6	3.9	3
ME49-4A1		Y	Perp	30	0/6										
ME49-5A1		Y	Perp	30	15/17	0.47	0.90	0.03	14.10	0.988	4/6	0/6	14.7	1.0	3

Table B.2
Individual microwave palaeointensity results from the AS section, La Palma. All column headings are explained in the caption to Table B.1.

Sample	Flow number	Demag	Protocol	F_{lab}	n/N	f	g	β	q	r^2	pT_MRM check	Tail check	F (μT)	Uncert (μT)	Class
AS3-5B1	3	Y	Coe	20	0/12										
AS4-4B1	4	Y	Coe	20	0/17										
AS4-4B2		Y	Perp	20	0/4										
AS4-4B3		Y	Perp	20	15/15	0.90	0.47	0.02	28.45	0.993	5/5	5/5	35.4	0.9	1
AS4-4B4		Y	Perp	20	0/24										
AS5-1A1	5	Y	Coe	20	0/11										
AS7-5B1	7	N													
AS8-2B1	8	Y	Perp	20	11/18	0.32	0.87	0.03	7.90	0.989	3/4	1/4	16.0	2.0	3
AS8-3B1		Y	Coe	20	7/7	0.39	0.78	0.07	4.50	0.977	1/3	3/3	15.8	3.5	3
AS8-3B2		Y	Coe	10	15/15	0.85	0.91	0.02	36.37	0.994	7/7	2/7	19.4	0.5	2
AS8-3B3		Y	Perp	20	0/10										
AS8-5B1		Y	Quasi	10	0/17										
AS9-1B1	9	Y													
AS10-U1	10	N													
AS10-U5		N													
AS11-2B1	11	Y	Quasi	1	0/8										
AS12-1B1	12	Y	Quasi	10	9/9	0.42	0.65	0.09	2.88	0.939	N/A	N/A	1.77	0.614	3
AS12-1B2		Y	Quasi	1	7/7	0.43	0.77	0.09	3.62	0.959	N/A	N/A	2.85	0.7864889	3
AS12-2B1		Y	Quasi	5	0/9										
AS12-3B1		N	Coe												
AS12-3B2		Y	Quasi	5	0/8										
AS12-4B1		Y	Quasi	5	5/9	0.69	0.73	0.04	13.90	0.996	N/A	N/A	4.3	0.3	2
AS12-5B1		Y	Quasi	1	0/8										
AS13-B1	13	Y	Coe	10	0/13										
AS14-U1	14	Y	Coe	20	7/14	0.46	0.80	0.06	6.45	0.984	3/3	3/3	10.38	1.60955	2
AS14-U2		Y	Perp	10	0/9										
AS14-U3		Y	Quasi	10	14/15	0.97	0.87	0.03	31.53	0.991	N/A	N/A	13.2	0.4	2
AS14-1B1		Y	Coe	10	7/13	0.52	0.78	0.04	9.14	0.990	3/4	4/4	5.75	0.629	2
AS14-2A1		Y	Perp	20	12/12	0.48	0.83	0.04	9.49	0.982	3/4	1/5	10.7	1.1	2
AS16-2B1	16	N													
AS16-4B1		Y													
AS15-1B1	15	Y	Coe	20	0/15										
AS15-1B2		Y	Quasi	10	13/13	0.74	0.84	0.06	9.69	0.955	N/A	N/A	7.9	0.8	3
AS15-1B3		Y	Quasi	5	7/17	0.66	0.78	0.04	12.02	0.990	N/A	N/A	14.7	1.2	2
AS15-2B1		Y	Coe	20	5/6	0.52	0.65	0.06	5.68	0.989	2/2	0/2	24.8	4.4	3
AS15-3B1		Y	Perp	20	5/6	0.08	0.66	0.04	1.14	0.994	0/2	0/2	17.9	15.6	3
AS14-1B1	14	Y	Coe		0/18										
AS14-1B2		Y	Coe	20	10/12	0.45	0.88	0.08	5.17	0.953	5/5	4/5	11.7	2.3	3
AS14-1B3		Y	Quasi	10	6/16	0.26	0.73	0.08	2.38	0.975	N/A	N/A	14.1	5.9	3
AS14-1B4		Y	Quasi	10	7/11	0.28	0.68	0.08	2.35	0.967	N/A	N/A	15.3	6.5	3
AS14-3B5		Y	Quasi	5	9/14	0.58	0.73	0.02	19.21	0.997	N/A	N/A	4.3	0.2	2
AS14-3B6		Y	Quasi	5	5/9	0.23	0.73	0.08	2.18	0.982	N/A	N/A	27.7	12.7	3
AS13-2B1	13	Y	Perp	20	11/11	0.60	0.81	0.02	22.72	0.996	4/4	2/4	18.1	0.8	2
AS13-3B1		Y	Coe	10	0/15										
AS13-3B2		Y	Coe	20	0/8										
AS13-3B3		Y	Quasi	10	6/6	0.23	0.74	0.03	5.05	0.994	N/A	N/A	3.3	0.6	3
AS13-3B4		Y	Quasi	10	9/9	0.73	0.82	0.02	31.46	0.997	N/A	N/A	2.4	0.1	2
AS13-3B5		Y	Quasi	10	9/9	0.87	0.79	0.04	15.46	0.986	N/A	N/A	2.6	0.2	2
AS13-3B6		Y	Quasi	10	11/21	0.45	0.83	0.08	4.94	0.949	N/A	N/A	21.0	4.3	3
AS13-3B7		Y	Quasi	10	7/15	0.54	0.78	0.04	10.25	0.992	N/A	N/A	4.5	0.4	2
AS13-3B8		Y	Quasi	10	14/14	0.75	0.85	0.04	15.06	0.979	N/A	N/A	4.1	0.3	3
AS13-3B9		Y	Perp	10	10/12	0.69	0.76	0.06	8.16	0.967	1/5	3/5	4.2	0.5	3
AS13-3B10		Y	Perp	10	12/20	0.53	0.79	0.01	39.61	0.999	0/0	0/0	4.6	0.1	2
AS13-3B11		Y	Perp	10	9/9	0.68	0.80	0.05	11.71	0.985	1/3	2/3	3.7	0.3	2
AS13-4B1		Y	Coe	20	12/26	0.48	0.88	0.03	14.74	0.991	4/5	5/5	6.5	0.4	2
AS13-4B2		Y	Perp	20	15/16	0.61	0.87	0.01	18.36	0.989	4/7	1/7	7.8	0.4	2
AS12-2B1	12	Y	Perp	10	7/9	0.58	0.45	0.40	6.51	0.992	2/3	0/3	2.2	0.3	3
AS12-2B2		Y	Perp	5	10/10	0.53	0.83	0.02	19.88	0.996	2/4	4/4	2.2	0.1	2
AS12-2B3		Y	Perp	5	9/13	0.42	0.80	0.05	6.36	0.980	3/5	3/4	4.2	0.7	3
AS12-2B4		Y	Perp	5	15/15	0.39	0.85	0.05	7.27	0.973	3/7	2/7	1.1	0.2	3
AS12-4B1		Y	Quasi	5	6/10	0.65	0.77	0.08	6.44	0.975	N/A	N/A	8.5	1.3	3

Table B.3
Individual microwave palaeointensity results from the AN section, La Palma. Flows are in stratigraphic order in ascending number from oldest to youngest. All column headings are explained in the caption to Table B.1.

Sample	Flow number	Demag	Protocol	F_{lab}	n/N	f	g	β	q	r^2	pT_MRM check	Tail check	F (μT)	Uncert (μT)	Class
AN1-1B1	1	Y	Perp	10	0/4										
AN1-1B2		Y	Perp	15	10/10	0.54	0.56	0.11	2.88	0.912	1/2	1/2	2.5	0.9	3
AN1-1B3		Y	Perp	2	0/9										
AN1-2A1		Y	Perp	15	0/3										
AN1-2A2		Y	Perp	4	6/7	0.38	0.40	0.14	1.07	0.920	0/1	0/1	3.2	3.0	3
AN1-4A1		Y	Perp	5	0/3										
AN1-5A1		Y	Perp	5	9/9	0.41	0.61	0.08	3.20	0.958	1/1	0/1	1.6	0.5	3
AN2-1B1	2	Y	Coe	40	0/4										
AN2-1B2		Y	Perp	10	6/6	0.63	0.71	0.02	20.86	0.998	1/1	1/2	7.5	0.4	2
AN2-2B1		Y	Coe	40	5/5	0.43	0.56	0.08	2.88	0.979	1/3	2/3	11.7	4.1	3
AN3-1B1	3	Y	Perp	10	7/8	0.39	0.67	0.09	2.93	0.961	2/2	0/2	4.6	1.6	3
AN3-1B2		Y	Perp	10	13/13	0.60	0.85	0.03	19.91	0.993	3/3	0/3	3.2	0.2	2
AN3-1B3		Y	Perp	10	5/5	0.53	0.68	0.04	8.85	0.995	0/1	1/1	6.6	0.7	2
AN3-2B1		Y	Coe	20	0/4										
AN3-3B1		Y	Perp	10	7/8	0.39	0.34	0.04	3.64	0.993	0/1	0/1	8.8	2.4	3
AN3-3B2		Y	Perp	10	8/8	0.38	0.70	0.04	6.50	0.990	1/2	2/2	11.5	1.8	2
AN4-1B1	4	Y	Coe	10	0/6										
AN4-2B1		Y	Coe	10	0/7										
AN4-3B1		Y	Perp	10	0/7										
AN4-4B1		Y	Perp	10	0/11										
AN6-1B1	6	Y	Perp	10	6/8	0.69	0.61	0.03	15.16	0.997	1/1	0/1	4.8	0.3	2
AN7-2B1	7	Y	Perp	10	3/4	0.28	0.35	0.03	3.53	0.999	0/0	0/0	13.9	3.9	3
AN7-3B1		Y	Perp	10	6/6	0.27	0.45	0.05	2.57	0.991	1/1	0/1	10.7	4.2	3
AN7-4B1		Y	Coe	30	0/5										
AN7-4B2		Y	Quasi	30	0/6										
AN8-2B1	8	Y	Perp	10	8/8	0.31	0.62	0.12	1.66	0.918	0/1	1/1	3.4	2.1	3
AN8-2B2		Y	Perp	10	10/10	0.53	0.56	0.07	4.13	0.958	1/2	0/2	5.1	1.2	3
AN8-2B3		Y	Quasi	10	5/5	0.80	0.74	0.05	12.66	0.993	N/A	N/A	3.7	0.3	2
AN8-3B1		Y	Perp	20	7/7	0.22	0.75	0.04	4.05	0.992	0/1	0/1	8.8	2.2	3
AN9A-1B1	9	Y	Perp	10	10/10	0.77	0.59	0.02	22.07	0.997	0/0	0/0	21.6	1.0	2
AN9A-2B1		Y	Perp	10	9/10	0.19	0.84	0.04	4.34	0.990	0/0	0/0	24.2	5.6	3
AN9A-3B1		Y	Perp	20	9/9	0.39	0.75	0.04	8.16	0.991	0/1	0/1	26.8	3.3	2
AN9A-4B1		Y	Perp	20	15/15	0.40	0.64	0.02	10.10	0.992	0/0	0/0	18.5	1.8	2
AN9B-4B1	10	Y	Perp	10	0/12										
AN10-1B1	11	N													
AN10-2B1		N													
AN10-3B1		N													
AN11-1B1	12	Y	Perp	10	3/3	0.73	0.50	0.09	4.13	0.992	1/1	1/1	31.7	7.7	3

Table B.4
Individual microwave palaeointensity results from Guadeloupe, French West Indies. Column headings are explained in Table B.1.

Sample	Flow number	Demag	Protocol	F_{lab}	n/N	f	g	β	q	r^2	pT_MRM check	Tail check	F (μT)	Uncert (μT)	Class
GD0102	1	Y	Perp	10	0/12										
GD0103		Y	Perp	20	0/8										
GD0104		Y	Coe	20	0/9										
GD0105		Y	Quasi	10	8/8	0.43	0.83	0.03	13.10	0.995	N/A	N/A	25.1	1.9	2
GD0106		Y	Quasi	20	11/12	0.51	0.89	0.02	19.15	0.995	N/A	N/A	19.1	1.0	2
GD0201		Y	Perp	30	0/8										
GD0301		Y	Perp	10	0/12										
GD0601		Y	Perp	10	0/9										
G01A0101	2	Y	Perp	6	0/9										
G01A0201		Y	Perp	6	8/10	0.41	0.71	0.10	2.89	0.940	1/2	0/2	4.2	1.5	3
G01A0401		Y	Perp	6											
G01A0402		Y	Perp	6	0/16										
G01A0501		Y	Perp	10	9/11	0.37	0.77	0.04	7.57	0.990	0/3	0/3	6.2	0.8	3
G01A0601		Y	Perp	6	7/9	0.31	0.75	0.16	1.42	0.870	0/1	0/1	5.2	3.6	3
G01A0701		Y	Perp	6	0/10										
G01B0102		Y	Perp	6	0/4										
G01B0201		Y	Perp	6	6/6	0.20	0.57	0.05	2.17	0.989	0/0	0/0	7.0	3.2	3
G01B0301		Y	Perp	6	0/9										
G01B0302		Y	Perp	6	0/9										
G01B0401		Y	Perp	6	7/7	0.73	0.72	0.05	10.48	0.987	0/1	1/1	3.0	0.3	2

Table B.4 (*Continued*)

Sample	Flow number	Demag	Protocol	F_{lab}	n/N	f	g	β	q	r^2	pT_MRM check	Tail check	F (μT)	Uncert (μT)	Class
G01B0402		Y	Perp	6	0/11										
G01B0501		Y	Perp	6	0/3										
G02A0101	3	Y	Perp	10	0/10										
G02A0201		Y	Perp	5	4/5	0.31	0.33	0.07	1.48	0.990	0/0	0/0	17.2	11.6	3
G02A0501		Y	Perp	10	0/5										
G02A0701		Y	Perp	20	0/12										
G02A0801		Y	Perp	10	0/4										
G02A0901		Y	Perp	5	7/7	0.26	0.75	0.09	2.26	0.963	0/1	0/1	7.8	3.5	3
G02A0902		Y	Perp	10	0/15										
G02B0101		Y	Perp	10	4/6	0.17	0.41	0.04	1.91	0.996	0/1	1/1	16.6	8.7	3
G02B0102		Y	Perp	10	5/5	0.46	0.72	0.04	8.95	0.996	1/1	1/1	17.0	1.9	2
G03A0101	4	Y	Perp	10	15/15	0.66	0.90	0.02	23.86	0.992	3/4	0/4	14.0	0.6	3
G03A0102		Y	Perp	20	11/11	0.84	0.81	0.03	21.56	0.991	0/3	0/1	15.4	0.7	3
G03A0201		Y	Perp	10	13/13	0.70	0.87	0.02	34.58	0.997	4/4	0/4	18.9	0.5	2
G03A0301		Y	Perp	15	0/13										
G03A0401		Y	Perp	15	10/10	0.71	0.61	0.04	9.90	0.985	0/2	0/2	19.7	2.0	3
G03A0501		Y	Perp	15	0/10										
G03A0502		Y	Perp	20	11/11	0.51	0.74	0.03	13.33	0.993	1/2	1/2	26.5	2.0	2
G03A0601		Y	Perp	15	8/8	0.44	0.64	0.04	6.86	0.990	2/2	0/2	15.7	2.3	2
G03A0701		Y	Perp	15	0/6										
G03A0801		Y	Perp	15	12/12	0.34	0.80	0.05	5.90	0.979	0/1	0/1	13.2	2.2	3
G03A0802		Y	Perp	20	5/17	0.13	0.51	0.16	1.26	0.992	1/2	0/2	10.8	8.6	3

References

Ancochea, E., Hernán, F., Cendrero, A., Cantagrel, J.M., Fúster, J.M., Ibarrola, E., Coello, J., 1994. Constructive and destructive episodes in the building of a young Oceanic Island, La Palma, Canary Islands and genesis of the Caldera de Taburiente. J. Volcanol. Geotherm. Res. 60, 243–262.

Aubert, J., Aurnou, J., Wicht, J., 2008. The magnetic structure of convection-driven numerical dynamos. Geophys. J. Int. 172, 945–956.

Barton, C.E., McFadden, P.L., 1996. Inclination shallowing and preferred transitional VGP paths. Earth Planet. Sci. Lett. 140, 147–157.

Biggin, A.J., Perrin, M., Dekkers, M.J., 2007a. A reliable absolute palaeointensity determination obtained from a non-ideal recorder. Earth Planet. Sci. Lett. 257, 545–563.

Biggin, A.J., Perrin, M., Shaw, J., 2007b. A comparison of a quasi-perpendicular method of palaeointensity determination with other thermal and microwave techniques. Earth Planet. Sci. Lett. 257, 564–581.

Blanc, F., 1983. Corrélations chronologiques et géochemique des formations volcanique du sud de la Basse-Terre, Guadeloupe (Petites Antilles). Début du cycle récent, 3e cycle thesis, Univ. Sci. Medic. Grenoble.

Bleil, U., Petersen, N., 1982. Magnetic properties of natural samples. In: Angenheister, G. (Ed.), Numerical Data and Functional Relationships in Science and Technology, Group V: Geophysics and Space Research. Springer, New York.

Brown, L.L., Pickens, J., Singer, B., 1994. Matuyama–Brunhes transition recorded in lava flows of the Chilean Andes: evidence for dipolar fields during reversals. Geology 22, 299–302.

Brown, L.L., Singer, B.S., Pickens, J.C., Jicha, R., 2004. Paleomagnetic directions and $^{40}Ar/^{39}Ar$ ages from the Tatara-San Pedro volcanic complex, Chilean Andes: Lava record of a Matuyama–Brunhes precursor? J. Geophys. Res. 109, B12101, doi:10.1029/2004JB003007.

Brown, M.C., Holme, R., Bargary, A., 2007. Exploring the influence of the non-dipole field on magnetic records for reversals and excursions. Geophys. J. Int. 168, 541–550.

Brown, M.C., Shaw, J., Goguitchaichvili, A.T., 2006. Microwave palaeointensity from the R3-N3 geomagnetic field reversal. Geophys. J. Int. 167, 53–69.

Butler, R.F., 1992. Paleomagnetism: Magnetic Domains to Geologic Terrains. Blackwell Science.

Carlut, J., Quidelleur, X., Courtillot, V., Boudon, G., 2000. Paleomagnetic directions and K/Ar dating of 0 to 1 Ma lava flows from La Guadeloupe Island (French West Indies: Implications for time-averaged field models. J. Geophys. Res. 105, 835–849.

Carlut, J., Quidelleur, X., 2000. Absolute paleointensities recorded during the Brunhes chron at La Guadeloupe Island. Phys. Earth Planet. Inter. 120, 255–269.

Carmichael, I.S.E., Nicolls, J., 1967. Iron-titanium oxides and oxygen fugacities in volcanic rocks. J. Geophys. Res. 72, 4665–4687.

Carracedo, J.C., Badiola, E.R., Guillou, H., Paterne, M., Scaillet, S., Torrado, F.J.P., Paris, R., Fra-Paleo, U., Hansen, A., 2007. Eruptive and structural history of Teide Volcano and rift zones of Tenerife, Canary Islands. Geol. Soc. Am. Bull. 119, 1027–1051, doi:10.1130/B26087.1.

Carracedo, J.C., Day, S.J., Guillou, H., Gravestock, P., 1999. Later stages of volcanic evolution of La Palma, Canary Islands: rift evolution, giant landslides, and the genesis of the Caldera de Taburiente. Geol. Soc. Am. Bull. 111, 755–768.

Carracedo, J.C., Day, S., Guillou, H., Badiola, E.R., Canas, J.A., Pérez Torrado, F.J., 1998. Hot spot volcanism close to a passive continental margin: the Canary Islands. Geol. Mag. 5, 591–604.

Celaya, M., Clement, B., 1988. Inclination shallowing in deep sea sediments from the north atlantic. Geophys. Res. Lett. 15, 52–55.

Channell, J.E.T., Curtis, J.H., Flower, B.P., 2004. The Matuyama–Brunhes boundary interval (500–900 ka) in North Atlantic drift sediments. Geophys. J. Int. 158, 489–505.

Channell, J.E.T., Lehman, B., 1997. The last two geomagnetic polarity reversals recorded in high-deposition-rate sediment drifts. Nature 389, 712–715.

Chauvin, A., Roperch, P., Duncan, R.A., 1990. Records of geomagnetic reversals from volcanic islands of French Polynesia 2. Paleomagnetic study of a flow sequence (1.2–0.6 Ma) from the island of Tahiti and discussion of reversal models. J. Geophys. Res. 95, 2727–2752.

Clement, B.M., Kent, D.V., 1986. Geomagnetic polarity transition records from five hydraulic piston core sites in the north Atlantic. Init. Rep. Deep Sea Drill. Proj. 94, 831–852.

Clement, B.M., Kent, D.V., 1991. A southern hemisphere record of the Matuyama–Brunhes polarity reversal. Geophys. Res. Lett. 18, 81–84.

Clement, B.M., 2004. Dependence of the duration of geomagnetic polarity reversals on site latitude. Nature 428, 637–640.

Coe, R.S., Glen, J., 2004. The complexity of reversals. Timescales of the paleomagnetic field. Geophys. Monogr. Ser. 145, 221–232, doi:10.29/145GM16.

Coe, R.S., Grommé, S., Mankinen, E.A., 1978. Geomagnetic paleointensities from radiocarbon-dated lava flows on Hawaii and the question of the Pacific nondiple low. J. Geophys. Res. 83, 1740–1756.

Coe, R.S., Hongre, L., Glatzmaier, G.A., 2000. An examination of simulated geomagnetic reversals from a palaeomagnetic perspective. Philos. Trans. R. Soc. Lond. 358, 1141–1170.

Coe, R.S., Prévot, M., Camps, P., 1995. New evidence for extraordinary rapid change of the geomagnetic field during a reversal. Nature 374, 687–692.

Coe, R.S., Prévot, M., 1989. Evidence suggesting extremely rapid field variation during a geomagnetic reversal. Earth Planet. Sci. Lett. 92, 292–298.

Coe, R.S., Singer, B.S., Pringle, M.S., Zhao, X., 2004. Matuyama–Brunhes reversal and Kaikatsura event on Maui: palaeomagnetic directions, $^{40}Ar/^{39}Ar$ ages and implications. Earth Planet. Sci. Lett. 222, 667–684.

Coe, R.S., 1967. Paleo-intensities of the Earth's magnetic field determined from Tertiary and Quaternary rocks. J. Geophys. Res. 72, 3247–3262.

Constable, C., 1990. A simple statistical model for geomagnetic reversals. J. Geophys. Res. 95, 4587–4596.

Cottrell, R.D., Tarduno, J.A., 1999. Geomagnetic paleointensity derived from single plagioclase crystals. Earth Planet. Sci. Lett. 169, 1–5.

Day, R., Fuller, M., Schmidt, V.A., 1977. Hysteresis properties of Titanomagnetites: grain size and compositional dependence. Phys. Earth Planet. Inter. 13, 260–267.

Dekkers, M.J., Böhnel, H.N., 2006. Reliable absolute palaeointensities independent of magnetic domain state. Earth Planet. Sci. Lett. 248, 508–517.

Dinarès-Turell, J., Sagnotti, L., Roberts, A.P., 1999. Relative paleointensity from the Jaramillo Subchron to the Matuyama/Brunhes as recorded in a Mediterranean piston core. Earth Planet. Sci. Lett. 194, 327–341.

Dungan, M., Wulff, A., Thompson, R., 2001. Eruptive stratigraphy of the tatara-san pedro complex, 36°, southern volcanic zone, chilean andes: reconstruction method and implications for magma evolution at long-lived arc volcanic centers. J. Petrol. 42, 555–626.

Dunlop, D., 2002a. Theory and application of the Day plot (Mrs/Ms versus Hcr/Hc) 1. Theoretical curves and tests using titanomagnetite data. J. Geophys. Res. 107, 2056, doi:10.1029/2001JB000486.

Dunlop, D., 2002b. Theory and application of the Day plot (Mrs/Ms versus Hcr/Hc) 2. Application to data for rocks, sediments, soils. J. Geophys. Res. 107, 2057, doi:10.1029/2001JB000487.
Fabian, K., 2001. A theoretical treatment of palaeointensity determination experiments on rocks containing pseudo-single or multi domain magnetic particles. Earth Planet. Sci. Lett. 188, 45–58.
Fisher, R.A., 1953. Dispersion on a sphere. Proc. R. Soc. Lond. Ser. A 217, 295–305.
Fox, J.M.W., Aitken, M.J., 1980. Cooling-rate dependency of thermoremanent magnetisation. Nature 283, 462–463.
Fuller, M., Hasted, 1997. Magnetic fields of (1) bottom hole assemblies, (2) advanced piston core inner barrels and (3) inner shoes. In: Ocean Drilling Program, Initial Res. Leg, 166.
Glen, J.M.G., Coe, R., Liddicoat, J., 1994. Persistent features of polarity transition records from western North America. Geophys. Res. Lett. 21, 1165–1168.
Glen, J.M.G., Valet, J.-P., Soler, V., Renne, P.R., Elmaleh, A., 2003. A Neogene geomagnetic polarity transition record from lavas of the Canary Islands, Spain: episodic volcanism and/or metatable transitional fields? Geophys. J. Int. 154, 426–440.
Goren-Inbar, N., Feibel, C.S., Verosub, K.L., Melamed, Y., Kislev, M.E., Tchernov, E., Saragusti, I., 2000. Pleistocene milestones on the Out-of-Africa corridor at Gescher Benot Ya'aqov, Israel. Science 289, 944–947.
Gratton, M.N., Goguitchaichvili, A., Conte, G., Shaw, J., Urrutia-Fucugauchi, J., 2005a. Microwave palaeointensity study of the Jorullo volcano (Central Mexico). Geophys. J. Int. 161, 627–634.
Gratton, M.N., Shaw, J., Brown, L.L., 2007. Absolute palaeointensity variations during a precursor to the Matuyama–Brunhes transition recorded in Chilean lavas. Phys. Earth Planet. Inter. 162, 61–72.
Gratton, M.N., Shaw, J., Herrero-Bervera, E., 2005b. An absolute palaeointensity record from SOH1 lava core, Hawaii using the microwave technique. Phys. Earth Planet. Inter. 148, 193–214.
Gubbins, D., 1999. The distinction between geomagnetic excursions and reversals. Geophys. J. Int. 137, F1–F2.
Guillou, H., Carracedo, J.C., Day, S.J., 1998. Dating of the upper Pleistocene Holocene volcanic activity of La Palma using the unspiked K-Ar technique. J. Volcanol. Geotherm. Res. 86, 137–149.
Guillou, H., Carracedo, J.C., Duncan, R.A., 2001. K-Ar, $^{40}Ar/^{39}Ar$ ages and magnetostratigraphy of Brunhes and Matuyama lava sequences from La Palma Island. J. Volcanol. Geotherm. Res. 106, 175–194.
Halgedahl, S.L., Day, R., Fuller, M., 1980. The effect of cooling rate on the intensity of weak-field TRM in single-domain magnetite. J. Geophys. Res. 85, 3690–3698.
Hartl, P., Tauxe, L., 1996. A precursor to the Matuyama/Brunhes transition-field instability as recorded in pelagic sediments. Earth Planet. Sci. Lett. 138, 121–135.
Hill, M.J., Gratton, M.N., Shaw, J., 2002a. A comparison of thermal and microwave palaeomagnetic techniques using lava containing laboratory induced remanence. Geophys. J. Int. 151, 157–163.
Hill, M.J., Gratton, M.N., Shaw, J., 2002b. Palaeomagnetic investigation of Tertiary lava from Barrington Tops, NSW, Australia, using thermal and microwave techniques. Earth Planet. Sci. Lett. 198, 245–256.
Hill, M.J., Shaw, J., Herrero-Bervera, E., 2005. Palaeointensity record through the Lower Mammoth reversal from the Waianae volcano, Hawaii. Earth Planet. Sci. Lett. 230, 255–272.
Hill, M.J., Shaw, J., 1999. Palaeointensity results for historic lavas from Mt Etna using microwave demagnetization/remagnetization in a modified Thellier-type experiment. Geophys. J. Int. 139, 583–590.
Hill, M.J., Shaw, J., 2007. The use of the 'Kono perpendicular applied field method' in microwave palaeointensity experiments. Earth Planets Space 59, 711–716.
Hoffman, K.A., Singer, B.S., 2004. Regionally recurrent paleomagnetic transitional field and mantle processes. Timescales of the paleomagnetic field. Geophys. Monogr. Ser. 145, 233–243, doi:10.29/145GM16.
Hoffman, K.A., 1992. Dipolar reversal states of the geomagnetic field and core-mantle dynamics. Nature 359, 789–794.
Hoffman, K.A., 1996. Transitional paleomagnetic field behavior: preferred paths or patches? Surv. Geophys. 17, 207–211.
Holik, J.S., Rabinowitz, P.D., Austin, J.A., 1991. Effects of Canary Island volcanism on structure of oceanic crust of Marocco. J. Geophys. Res. 96, 12039–12067.
Johnson, C.L., Wijbrans, J.R., Constable, C.G., Gee, J., Staudigel, H., Tauxe, L., Forjaz, V.-H., Salgueiro, M., 1998. $^{40}Ar/^{39}Ar$ ages and paleomagnetism of São Miguel lavas, Azores. Earth Planet. Sci. Lett. 160, 637–649.
Kirschvink, J.L., 1980. The least-squares line and the plane and the analysis of palaeomagnetic data. Geophys. J. R. Astron. Soc. 62, 699–718.
Komorowski, J.-C., Boudon, G., Semet, M., Beauducel, F., Antenor-Habazac, C., Bazin, S., Hammouya, G., 2005. Guadeloupe. In: Lindsay, J.M., Robertson, R.E.A., Shepherd, J.B., Ali, S. (Eds.), Volcanic Hazard Atlas of the Lesser Antilles. Seismic Res Unit, Univ West Indies.
Kono, M., Ueno, N., 1977. Paleointensity determination by a modified Thellier method. Phys. Earth Planet. Inter. 13, 305–314.
Korte, M., Constable, C.G., 2005. Continuous geomagnetic field models for the past 7 millenia: 2. CALS7K. Geochem. Geophys. Geosyst. 6, Q02H16, doi:10.1029/2004GC000801.
Langereis, C.G., van Hoof, A.A.M., Rochette, P., 1992. Longitudinal confinement of geomagnetic reversal paths as a possible sedimentary artefact. Nature 358, 226–230.
Lattard, D., Engelmann, R., Kontny, A., Sauerzapf, U., 2006. Curie temperatures of synthetic titanomagnetites in the Fe–TI–O system: effects of composition, crystal chemistry, and thermomagnetic methods. J. Geophys. Res. 111, B12S28, doi:10.1029/2006JB004591.
Leonhardt, R., Fabian, K., 2007. Paleomagnetic reconstruction of the global geomagnetic field evolution during the Matuyama/Brunhes transition: iterative Bayesian inversion and independent verification. Earth Planet. Sci. Lett. 253, 172–195.
Leonhardt, R., Matzka, J., Nichols, A.R.L., Dingwell, D.B., 2006. Cooling rate correction of paleointensity determination for volcanic glasses by relaxation geospeedometry. Earth Planet. Sci. Lett. 243, 282–292.
Lin, J.L., Verosub, K.L., Roberts, A.P., 1994. Decay of the virtual dipole moment during polarity transitions and geomagnetic excursions. Geophys. Res. Lett. 21, 525–528.
Mankinen, E.A., Prévot, M., Grommé, C.S., Coe, R.S., 1985. The Steens Mountain (Oregon) geomagnetic polarity transition 1. Directional history, duration of episodes, and rock magnetism. J. Geophys. Res. 90 (B12), 10393–10416.
McArdle, N.J., Halls, H.C., Shaw, J., 2004. Rock magnetic and a comparison between microwave and Thellier palaeointensities for Precambrian dykes. Phys. Earth Planet. Inter. 147, 247–254.
Merrill, R.T., McFadden, P.L., 1999. Geomagnetic polarity reversals. Rev. Geophys. 37 (2), 201–226.
Meynadier, L., Valet, J.-P., Bassinot, F.C., Shackleton, N.J., Guyodo, N.J., 1994. Asymmetrical saw-tooth pattern of the geomagnetic field intensity from equatorial sediments in the Pacific and Indian Oceans. Earth Planet. Sci. Lett. 126, 109–127.
Mochizuki, N., Tsunakawa, H., Kurata, M., Yamazaki, T., Oda, H., 2005. Palaeointensity study of the Brunhes–Matuyama polarity reversal recorded in the lava sequence in Punaruu valley, Tahiti Island. 10th Scientific Assembly of the IAGA, IAGA2005-A-01158.
Moskowitz, B.M., Jackson, M., Kissel, C., 1998. Low-temperature magnetic behavior of titanomagnetites. Earth Planet. Sci. Lett. 157, 141–149.
Moskowitz, B.M., 1981. Methods for estimating Curie temperatures of titanomaghemites from experimental Js-T data. Earth Planet. Sci. Lett. 52, 84–88.
Nagata, T., Arai, Y., Momose, K., 1963. Secular variation of the geomagnetic force during the last 5000 years. J. Geophys. Res. 68, 5277–5281.
Navarro, J.M., Coello, J., 1993. Geological map of the national park of the Caldera de Taburiente, vol. 1 of 1. Instituto Nacional para la Conservacion de la Naturaleza, La Palma.
Olsen, N., Lühr, H., Sabaka, T.J., Mandea, M., Rother, M., Tøffner-Clausen, L., Choi, S., 2006. CHAOS—a model of the Earth's magnetic field derived from CHAMP, ørsted, and SAC-C magnetic satellite data. Geophys. J. Int. 166 (1), 65–75.
Olson, P., Amit, H., 2006. Changes in earth's dipole. Naturwissenschaften 93, 519–542.
Özdemir, O., Dunlop, D.J., Moskowitz, B.M., 1993. The effect of oxidation on the Verwey transition in magnetite. Geophys. Res. Lett. 20, 1671–1674.
Perrin, M., Schnepp, E., 2004. Iaga paleointensity database: distribution and quality of the data set. Phys. Earth Planet. Inter. 147, 255–267.
Petronille, M., Goguitchaichvili, A., Henry, B., Alva-Valdivia, L.M., Rosas-Elguera, J., Urrutia-Fucugauchi, J., Cejá, M.R., Calvo-Rathert, M., 2005. Paleomagnetism of Ar-Ar dated lava flows from the Caboruco-San Pedro volcanic field (western Mexico): evidence for the Matuyama–Brunhes transition precursor and a fully reversed geomagnetic event in the Brunhes chron. J. Geophys. Res. 110, B08101, doi:10.1029/2004JB003321.
Prægel, N.O., Holm, P.M., 2006. Lithospheric contributions to high MgO basanites from the Cumbre Vieja volcano, La Palma, Canary Islands and evidence for temporal variation in plume influence. J. Volcanol. Geotherm. Res. 149, 213–239.
Quidelleur, X., Carlut, J., Gillot, P.-Y., Soler, V., 2002. Evolution of the geomagnetic field prior to the Matuyama–Brunhes transition: radiometric dating of a 820 ka excursion at La Palma. Geophys. J. Int. 151, F6–F10.
Quidelleur, X., Carlut, J., Soler, V., Valet, J.-P., Gillot, P.-Y., 2003. The age and duration of the Matuyama–Brunhes transition from new K-Ar data from La Palma (Canary Islands) and revisited $^{40}Ar/^{39}Ar$. Earth Planet. Sci. Lett. 208, 149–163.
Quidelleur, X., Gillot, P.-Y., Carlut, J., Courtillot, V., 1999. Link between excursions and palaeointensity inferred from abnormal field directions recorded at La Palma around 600 ka. Earth Planet. Sci. Lett. 168, 233–242.
Quidelleur, X., Valet, J.-P., 1996. Geomagnetic changes across the last reversal recorded in lava flows from La Palma, Canary Islands. J. Geophys. Res. 101, 13,755–13773,13773.
Raisbeck, G.M., Yiou, F., Cattani, O., Jouzel, J., 2006. ^{10}Be evidence for the Matuyama–Brunhes geomagnetic reversal in the EPICA Dome C ice core. Nature 44, 82–84.
Riisager, P., Riisager, J., 2001. Detecting multidomain magnetic grains in Thellier palaeointensity experiments. Phys. Earth Planet. Inter. 125, 111–117.
Rolph, T.C., Shaw, J., 1985. A new method of paleofield magnitude correction for thermally altered samples and its application to Lower Carboniferous lavas. Geophys. J. R. Astr. Soc. 80, 773–781.
Samper, A., Quidelleur, X., Lahitte, P., Mollex, D., 2007. Timng of effusive volcanism and collapse events within an oceanic arc island: Guadeloupe archipelago (Lesser Antilles Arc). Earth Planet. Sci. Lett. 258, 175–191.
Schneider, D.A., Kent, D.V., Mello, G.A., 1992. A detailed chronology of the Australian impact event, the Brunhes–Matuyama polarity reversal, and global climate change. Earth Planet. Sci. Lett. 111, 395–405.
Selkin, P.A., Tauxe, L., 2000. Long-term variations in palaeointensity. Philos. Trans. R. Soc. Lond. A 358, 1065–1088.
Shao, J.C., Fuller, M., Tanimoto, T., Dunn, J.R., Stone, D., 1999. Spherical harmonic analyses of paleomagnetic data: the timeaveraged geomagnetic field for the past 5 Myr and the Brunhes–Matuyama reversal. J. Geophys. Res. 104, 5015–5030.
Shaw, J., Share, J.A., 2007. A new automated microwave demagnetiser/remagnetiser system for palaeointensity studies. Eos Trans. AGU Fall Meet. Suppl., Abstract, GP53C–1371.
Shaw, J., 1974. A new method of determining the magnitude of the palaeomagnetic field. Application to five historic lavas and five archaeological samples. Geophys. J. R. Astron. Soc. 39, 133–141.

Singer, B.S., Hoffman, K.A., Coe, R.S., Brown, L.L., B.R.J., Pringle, M.S., Chauvin, A., 2005. Structural and temporal requirements for geomagnetic field reversal deduced from lava flows. Nature 434, 633–636.

Singer, B.S., Relle, M.K., Hoffman, K.A., Battle, A., Laj, C., Guillou, H., Carracedo, J.C., 2002. Ar/Ar ages from transitionally magnetized lavas on La Palma, Canary Islands, and the geomagnetic instability timescale. J. Geophys. Res. 107, 2307, doi:10.1029/2001JB001613.

Smirnov, A.V., Tarduno, J.A., 2005. Thermochemical remanent magnetization in Precambrian rocks: are we sure the geomagnetic field was weak? J. Geophys. Res. 110, B06103, doi:10.1029/2004JB003445.

Staudigel, H., Feraud, G., Giannerini, G., 1986. The history of intrusive activity on the island of La Palma (Canary Islands). J. Volcanol. Geotherm. Res. 27, 299–322.

Tanaka, H., Kono, M., 1991. Preliminary results and reliability of paleointensity studies on historical and 14C dated Hawaiian lavas. J. Geomag. Geoelectr. 43, 375–388.

Tan, X., kodama, K.P., Gilder, S., Courtillot, V., 2007. Rock magnetic evidence for inclination shallowing in the Passaic Formation red beds from the Newark basin and a systematic bias of the Late Triassic apparent polar wander path for North America. Earth Planet. Sci. Lett. 254, 345–357.

Tarduno, J.A., Smirnov, A.V., 2004. The paradox of low field values and the long-term history of the geodynamo. Timescales of the paleomagnetic field. Geophys. Monogr. Ser. 145, 75–84, doi:10.29/145GM08.

Tauxe, L., Bertram, H.N., Seberino, C., 2002. Physical interpretation of hysteresis loops: Micromagnetic modeling of fine particle magnetite. Geochem. Geophys. Geosyst. 3 (10), 1055, doi:10.1029/2001GC000241.

Tauxe, L., Herbert, T., Shackleton, N.J., Kok, Y.S., 1996. Astronomical calibration of the Matuyama–Brunhes boundary: Consequences for magnetic remanence acquisition in marine carbonates and the Asian loess sequences. Earth Planet. Sci. Lett. 140, 133–146.

Tauxe, L., Kent, D.V., 2004. A simplified statistical model for the geomagnetic field and the detection of shallow bias in paleomagnetic inclinations: was the ancient magnetic field dipolar? Timescales of the paleomagnetic field. Geophys. Monogr. Ser. 145, 101–115, doi:10.29/145GM08.

Tauxe, L., Staudigel, H., Wijbrans, J.R., 2000. ^{40}Ar/ ^{39}Ar ages from La Palma in the Canary Islands. Geochem. Geophys. Geosyst. 1, 63.

Thellier, E., Thellier, O., 1959. Sur l'intensité du champ magnétique terrestre dans le passé historique et géologique. Ann. Géophys. 15, 285–376.

Valet, J.-P., Brassart, J., LeMeur, I., Soler, V., Quidelleur, X., Tric, E., Gillot, P.-Y., 1996. Absolute paleointensity and magnetomineralogical changes. J. Geophys. Res. 101, 25,029–25044,25044.

Valet, J.-P., Brassart, J., Quidelleur, X., Soler, V., Gillot, P.-Y., Hongre, L., 1999. Paleointensity variations across the last geomagnetic reversal at La Palma, Canary Islands, Spain. J. Geophys. Res. 104 (B4), 7577–7598.

Valet, J.-P., Kidane, T., Soler, V., Brassart, J., Courtillot, V., Meynadier, L., 1998. Remagnetization in lava flows recording pretransitional directions. J. Geophys. Res. 103, 9755–9775.

Valet, J.-P., Tauxe, L., Clark, D.R., 1988. The Matuyama–Brunhes transition recorded from Lake Tecopa sediments (California). Nature 315, 217–218.

Valet, J.-P., Tauxe, L., Clement, B., 1989. Equatorial and mid-latitude records of the last geomagnetic field reversal from the Atlantic Ocean. Earth Planet. Sci. Lett. 94, 371–384.

van Hoof, A.A.M., Vanos, B.J.H., Rademakers, J.G., Langereis, C.G., Delange, G.J., 1993. A paleomagnetic and geochemical record of the upper Cochiti reversal and two subsequent precessional cycles from southern Sicily (Italy). Earth Planet. Sci. Lett. 117, 235–250.

Verosub, K.L., Goren-Inbar, N., Feibel, C., Saragusti, I., 1998. Location of the matayuma/brunhes boundary in the gesher benot ya'aqov archaeological site, israel. Paleoanthropology Society Annual Meeting, Seatle. J. Hum. Evol. 34, A22.

Walton, D., Böhnel, H., Dunlop, D.J., 2004. 2d order ferromagnetic resonance in nanoparticles. Phys. Stat. Sol. 201, 3257–3262, doi:10.1002/pssa.200405435.

Walton, D., 2002. Conditions for ferromagnetic resonance in nanoparticles and microwave magnetization. Geophys. Res. Lett. 29, 2165, doi:10.1029/2002GL016049.

Walton, D., 2004a. Avoiding mineral alteration during microwave magnetization. Geophys. Res. Lett. 31, L03606, doi:10.1029/2003GL019011.

Walton, D., 2004b. Resetting the magnetization of assemblies of nanoparticles with microwaves. J. Appl. Phys. 95, 5247–5248, doi:10.1063/1.1695605.

Watts, A.B., 1994. Crustal structure, gravity anomalies and flexure of lithosphere in the vicinity of the Canary Islands. Geophys. J. Int. 119, 648–666.

Wicht, J., Olson, P., 2004. A detailed study of the polarity reversal mechanism in a numerical dynamo model. Geochem. Geophys. Geosyst. 5 (3), doi:10.1029/2003GC000602.

Wicht, J., 2005. Palaeomagnetic interpretation of dynamo simulations. Geophys. J. Int. 162, 371–380.

Yamamoto, Y., Tsunakawa, H., Shibuya, H., 2003. Palaeointensity study of the Hawaiian 1960 lava: implications for possible causes of erroneously high intensities. Geophys. J. Int. 153, 263–276.

Yamamoto, Y., Tsunakawa, H., 2005. Geomagnetic field intensity during the last 5 Myr: LTD-DHT Shaw palaeointensities from volcanic rocks of the Society Islands, French Polynesia. Geophys. J. Int. 162, 79–114.

Yamamoto, Y., 2006. Possible TCRM acquisition of the kilauea 1960 lava, Hawaii: failure of the Thellier paleointensity determination inferred from equilibrium temperature of the Fe-Ti oxide. Earth Planets Space 58, 1033–1044.

Yamazaki, T., Oda, H., 2001. A Brunhes–Matuyama polarity transition record from anoxic sediments in the South Atlantic (Ocean Drilling Program Hole 1082C). Earth Planets Space 53, 817–827.

Yu, Y., Tauxe, L., Genevey, A., 2004. Toward an optimal geomagnetic field intensity determination technique. Geochem. Geophys. Geosyst. 5 (2), Q02H07, doi:10.1029/2003GC000630.

Zhu, R., Liu, C., Wu, H., Zhu, G., 1991. Transitional field behaviour for the Matuyama–Brunhes. Sci. China Ser B 34, 1252–1257.